UNIVERSITÀ DEGLI STUDI DI PADOVA

DIPARTIMENTO DI INGEGNERIA INDUSTRIALE

NUMERICAL INVESTIGATION OF NOZZLE THERMOCHEMICAL BEHAVIOUR IN HYBRID ROCKET MOTORS

CORSO DI LAUREA MAGISTRALE IN INGEGNERIA AEROSPAZIALE

RELATORE: PROF. DANIELE PAVARIN
CORRELATORE: ING. FRANCESCO BARATO

LAUREANDO: ALESSANDRO RUFFIN

ANNO ACCADEMICO 2014-2015

Dedicated to my family

Mighty oaks from little acorns grow

- Old Saying

ABSTRACT

Solid and hybrid rocket motor nozzles are protected from the high enthalpy gasses using particular kind of materials that absorb the transferred thermal energy by changing their chemical state. This turns into a recession of nozzle surface called erosion.

In the past, during a nozzle design procedure, the throat erosion was predicted by scaling experimental data to the analysed case. This is allowed if thermochemical environments are alike. If a hybrid rocket motor nozzle is going to be designed the use of this scaling procedure can lead to an inaccurate design.

In this thesis work a physics-based model to predict nozzle thermochemical erosion is presented. This model is based on non-charring materials ablation phenomena and can be used to predict the erosion in the peculiar hybrid rocket motor environment and comparing different propellant compositions.

CONTENTS

x

LIST OF FIGURES

LIST OF TABLES

INTRODUCTION

1.1 HYBRID ROCKET MOTORS

Traditionally there are two main rocket motor configurations: liquid rocket motor and solid rocket motor (SRM[1]).

In bi-propellant liquid rocket motors, the hot gas flow is produced from the reaction between fuel and oxidizer which are stored in separate tanks. The reactants are pressurized and driven to the combustion chamber by a complex pumping system. Since, normally, the fuel is warmed in a regenerative fashion using nozzle heat fluxes the motor throttlability is limited. Bi-propellant pump pressure fed rocket engines are the most efficient and expensive chemical motors, 275-400 s is the typical specific impulse range.

Another kind of engine is the mono-propellant liquid motor where the high-enthalpy gas is obtained from the exothermic decomposition of the liquid propellant stored in a tank. This system is less performable than the bi-propellant one (I_{sp}=180-210 s) and so the system is used for small motors and generally is tank pressure fed. In order to reduce the friction loss no regenerative cooling nozzle is used, this significantly simplifies the motor. Mono-propellant liquid engines were the first to allow deep-throttling and so they suited purposes like soft lunar landing. Liquid rocket motors were historically considered safer than other engines and then they played a major role in the manned mission scenario.

In SRMs the gas flow is obtained from the reaction of the solid state fuel and oxidizer mixture called propellant grain. This is stored inside the combustion chamber and the combustion mechanism is auto-sustained, i.e. after ignition the combustion can not be controlled and stops only when there's no more propellant. Therefore an accurate design is paramount in order to predict the motor behaviour. In contrast, solid rocket motors are mechanically simpler than the liquid ones[2] and the specific impulse is still high (250-280 s). In particular the volumetric specific impulse is higher than the one achieved with the other motors, this suits them for completely different purposes like stage separation and ballistic missiles.

Both high performance liquid and solid rocket motors are affected by major disadvantages, the first ones are complex and expensive, the second ones lack direct control. A third chemical motor category that avoids major issues, maintaining high theoretical performance, is represented by hybrid rocket motors (HRM[3]).

---

1 Solid Rocket Motor
2 SRMs do not require valves and pumps.
3 Hybrid Rocket Motor
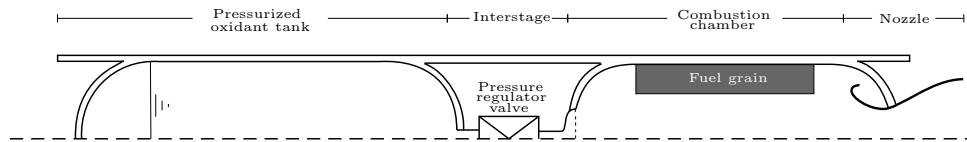
Figure 1: Hybrid rocket motor typical configuration

In HRMs liquid oxidizer is stored in a pressurized tank and solid state fuel grain is kept inside the combustion chamber as shown in figure 1. The oxidizer flow is controlled via a pressure regulator valve that makes the system able to slightly throttle and abort. These are main requirements for a safe motor. Motor ignition can be carried out with traditional igniter or, if a oxygen based mono-propellant is used, via oxidizer decomposition available heat. The latter ignition mechanism makes an HRM potentially restartable and so suited as a multi-purpose engine. To avoid pressure drop or oxidizer premature decomposition no regenerative technique is usually used and then nozzle and combustion chamber are protected from the thermal environment the same way as SRMs. As a result HRMs are much cheaper than liquid rocket engines and slightly more complex than SRMs. For their heterogeneous nature hybrid motors are less prone to explosion and fire hazard, this intrinsic safety allows to reduce development costs in addition to manufacturing costs.

There are few drawbacks anyway. While in a SRM reactants are premixed, and in a liquid engine they are forced to impinge together by the ignition plate, in HRMs the reaction mechanism is carried out in the boundary layer. The fuel grain melts or decomposes under the flame heat, the produced gases diffuse from the grain wall through the boundary layer, on the other side (the gas side) the oxidizing species diffuse through the boundary layer in direction of the fuel. The reacting species meet in a region where the local oxidant to fuel ratio makes the reaction possible and originates the flame[4]. The distance from the wall of the flame regulate the fuel recession rate since the melting and decomposition heat is received from the flame. Unfortunately, the decomposition gases blowing effect on the boundary layer tends to keep the flame away from the wall. This is known as *blocking effect* and is the cause of the HRM reduced burning rate. To avoid this issue different methods were used:

- Multiport fuel grains were the first solutions adopted in order to reduce the grain length, but this involves an excessive amount of slivers (unburned mass fraction);

---

4 This particular kind of flame is denoted as a diffusion limited flame

- The introduction of oxidizing additive to the fuel can be adopted, but this could reduce the safe nature of HRM;

- Fuels with the tendency to generate a liquid layer were introduced, under proper fluid dynamic conditions liquid droplet entrainment occurs. This is known as *entrainment effect* and is a way to rise the regression rate that led to development of paraffin and polyethylene wax fuel grains;

- Some devices can be introduced in order to increase the fluid dynamic effect on the combustion mechanism, these commonly are particular injectors or plates that induce turbulent path to the flow;

- Introduction of metal particles in fuel grain formulation to increase exhaust emissivity and then radiative heat flux.

Another fundamental aspect of HRMs is the sensitivity to system size and variation of oxidizer concentration through the combustion chamber length. The size is a characteristic parameter for fluid dynamics that affects wall heat transfer, this hinder reduced scale tests and make very large system difficult to design, i.e. difficulty in scaling the system. The reduction of oxidizer availability through the length makes the fuel, at the end of the grain, less prone to react and then post-combustion chamber design should be adequate for the mixing of reactants remnant.

Mixing of oxidizer and fuel is a critical aspect of hybrid engine, this and a reduced regression rate strongly affects combustion efficiency, then in present state of art liquid and solid rocket motors perform better than the hybrid ones. Since safety and low cost are HRM strong points is important that any research effort that will be made to increase combustion and overall efficiency won't compromise them.

Present hybrid rocket technology applications are sounding rockets, commercial manned space flights and cost-driven applications. Regarding commercial manned space flights the most common example are Virgin Galactic SpaceShipOne and SpaceShipTwo (both powered by hybrid rocket motors), in this case safety and cost are more important than performance. HRM could permit the development of a sustainable, low-cost, high launch frequency sounding rocket system aimed at scientific, commercial and educational purposes. Other possible applications are small launch vehicles and ballistic missiles, but traditional solutions are well rooted in this case.

Common use fuels are HTPB, polyethylene wax and paraffin. Low-cost, easily available, oxidizers are LOX, N_2O,and H_2O_2. There are anyway a lot of toxic oxidizers like IRFNA, N_2O_2 and fluorine, the latter can give outstanding performance.

Solid and hybrid rocket motors are normally protected from the high enthalpy environment using ablative materials. With these materials the convective and radiative heat from the exhaust gasses flow is mitigated via material mass loss caused by chemical reactions. There are two main ablative material categories: charring and non-charring.
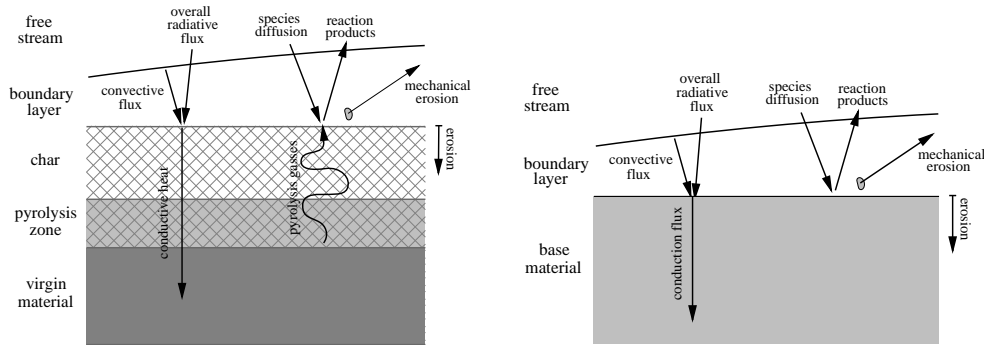
Figure 2: Charring and non-charring ablation mechanisms

Most charring ablative materials are reinforced plastics. When heated the polymeric base decomposes producing pyrolysis gasses and leaving a carbonaceous residue that bounds with the reinforcement. This porous heterogeneous solid mixture is denoted as *char*. The pyrolysis gasses flow in direction of the exposed surface through the previously formed char. Meanwhile the char is cooled by the pyrolysis gas. The free-stream reactive species diffuse trough the boundary layer and react with the char and the pyrolysis gasses at the nozzle wall. In this process char mass is lost due to the chemical reaction with the reactive species. The overall reaction heat at the surface must be endothermic in order to mitigate the convective and radiative heat fluxes that otherwise would be conducted by the char. At the surface other two secondary erosion mechanisms take place: mechanical spallation of the char and removal of the liquid phase residue. A lot of charring ablative materials were developed but experimental evaluations revealed that two of them were superior to the others: silica and carbon/graphite reinforced phenol-formaldehyde resins which are the most diffused charring ablative materials.

No in-depth decomposition or pyrolysis reactions take place in non-charring ablative materials and so, as the name suggests, no char is formed. The main events in these protection systems are the heterogeneous reactions between reactive species and base material or melting-sublimation at the surface. Mechanical spallation of the surface can occur, especially at the begin of the firing, when the radial thermal gradient are high. Commonly used

non-charring ablative materials are pyrolytic graphite, polycrystalline (bulk) graphite and carbon-carbon. All this materials are almost entirely made of carbon. At nearly 4000 K the carbon ablating behaviour changes, and at that temperature sublimation will occur. This is a highly endothermic phenomena that could make this material very efficient, but normally the nozzle wall doesn't reach the sublimation temperature and so chemical reaction with flow gasses is the main ablation contribute.

Non-ablative thermal protection behaviour in HRM environment is the object of study in this thesis work.

1.3 NOZZLE DESIGN

Rocket motor nozzle principal function is to convert the combustion chamber enthalpy into kinetic energy which provides most part of the needed thrust. Since in the nozzle the highest levels of flow speed are reached, this is the region where the most severe convective heat fluxes are applied to the wall.

Then it's important to find a way to mitigate and/or reduce these fluxes in order to protect the structural integrity of the component, and from what has been said in the previous section, it's evident that this is achieved in the same fashion used in SRMs, i.e. ablative thermal protections.

There is no standard procedure to design an HRM/SRM nozzle, but, for sure, the final design is obtained in a iterative way. The flow diagram in figure 3 illustrates the method presented in [2], which involves different subsystems and consists in two main loop.

The first step of the inner loop is the aerodynamic design, here the initial nozzle contour is defined in order to maximize the thrust coefficient, reduce the nozzle weight (which often means length) and the friction loss. In the second step, thermal design, a thickness profile is assigned to the inner thermal liner, this assignment is based on past designs or experience. Then the structure which should support the thermal liner and resist the pressure load is characterized.

The following two steps are needed to understand if the subsystem designs defined in the first three steps are up to the task. In step four, aerothermal analysis, given the nozzle initial geometry and the thermal liner thickness a simulation system, involving an adequate physical model, is used, to understand if there is too much or not enough thermal insulation to keep the support structure in the required temperature range, and if the surface erosion is acceptable. The structural analysis, step five, allows to find out whether the structural stiffness is acceptable and if it's possible to reduce the subsystem weight maintaining the structural stiffness and without buckling to occur.

Once an overall design that fulfil the requirement is achieved, within an adequate tolerance, it's possible to estimate the nozzle performance and
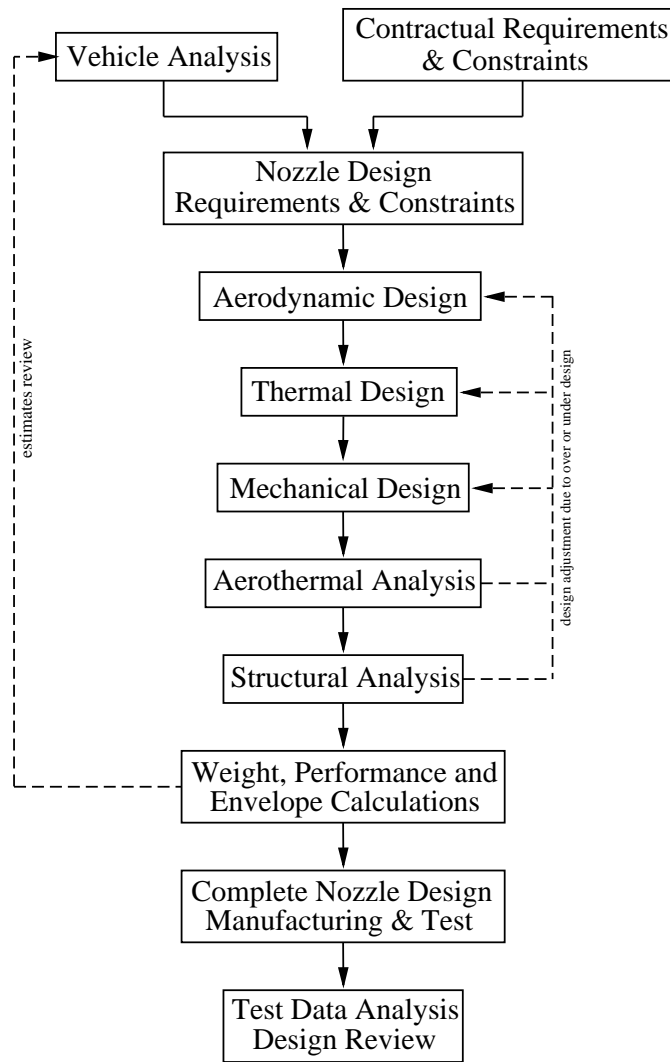
Figure 3: Nozzle Design Flow Diagram

weight. Those are compared with the initial estimations used in a previous vehicle flight analysis, via the outer iterative loop.

If the values match or convergence is reached, then the design is complete. The manufacturing and test phases follow, the latter proves if the design procedure was proper. In particular the aerothermal and structural analyses could be modified after test in order to achieve future better designs.

Since a rocket motor nozzle design is a complex process that involves knowledge in different engineering fields, this thesis will focus in thermal design and aerothermal analysis only. The needed aerodynamic outline will be based on successfully designed nozzles.

Thermal design consists in defining the thermal liner thickness, an initial concept can be obtained from successful nozzle designs or from designer experience. Following designs are defined from previous aerothermal analysis, in order to achieve the optimal and final thermal liner configuration. In this phase other manufacturing-related parameters are defined, for example composite lay-up angle and reinforcement volume fraction.

Aerothermal analysis goal is to obtain surface recession and in-depth temperature response. This can be carried out in different ways depending on the progress of overall nozzle design and the available time to conduct the design and test. The procedure involves the use of physical models, with an increasing level of detail, analysed with the use of several commercially available computer codes or a self-developed code.

A common procedure for this analysis can be represented by the following steps:

- for a given propellant and combustion chamber pressure use a thermochemical code to get the flow composition, and some flow properties;

- obtain other needed flow properties via temperature dependent functions and mixing laws;

- flow field characterization to acquire the film coefficient (or *Stenton Number*) and the diffusion coefficient, if possible or needed;

- apply the thermal design and obtained flow parameter to the physical model (i.e. ablation model) in order to get the surface erosion rate and in-depth thermal response;

- compare those results with available firing test data to estimate the process error or to get a more accurate physical model.

In some cases the flow characterization and the ablation model steps can be merged in order to achieve the best results with a given code. For example integrate the ablation model in a UDF[5] that will be applied in a CFD[6] code.

Very often the code used to obtain the flow composition is NASA's CEA[7], the code usage made during this thesis work will be explained further in chapter 2.

---

5 User Defined Function
6 Computational Fluid Dynamics
7 Chemical Equilibrium and Application

On the other hand there are many ways to obtain a film coefficient trend, from the simple *Bartz equation*, to a more complicate CFD program which probably has been commercially developed. Obviously the method choice depends on the actual state of the overall design. For what concerns the diffusion coefficient, there are mainly two approaches to acquire it. The first and historically one is based on the *Reynolds analogy* for close to unity *Lewis number*, the other one involves the use of CFD programs. These fluid flow aspects will be further investigate in chapter 3.

The ablation model can be implemented in a one-dimensional computer code such as Aerotherm's CMA[8], an axis-symmetric one like Aerotherm's ASCHAR[9] or a self-developed code. The comparison of the results with firing test data is not possible in first stages of the design, so ablation thermal validation with known tests is useful. Some particular material require the determination of the wall chemical composition, the Aerotherm's EST code can be used for this task. Anyway other methods that do not involve the equilibrium hypothesis are possible.

In this thesis work non-charring materials physics was evaluated, with particular interest in carbon based ablative materials and their behaviour in an HRM environment. In order to do this the phenomena modelling was implemented in a one-dimensional self-developed code, as explained in chapter 4.

The achievement of this thesis work are reported in the conclusive chapter 5.

---

8 Charring Material Thermal Response and Ablation
9 Axisymmetric Transient Heating and Material Ablation

THERMOCHEMICAL ENVIRONMENT CHARACTERIZATION

Thermochemical environment characterization is a main feature in understanding rocket motor performance and thermal protection system behaviour. From the performance point of view, chemical equilibrium codes are used to get the theoretical characteristic velocity, in fact with them it is possible to obtain indirectly the adiabatic flame temperature and the average molar weight. For most thermal protection, the free-stream chemical composition is needed in order to understand the way they will perform.

In this thesis work NASA's CEA computer program was used to obtain combustion chamber temperature and molar fraction of species present in the flow for a given combustion chamber pressure and oxidizer to fuel ratio (o/f). The chemical composition was then used to obtain flow thermodynamic properties.

Since in a rocket motor the pressure and o/f conditions are not constant a *MATLAB*® code aimed to obtain a look-up table was developed.

2.1 NASA'S CHEMICAL EQUILIBRIUM AND APPLICATIONS

NASA's Chemical Equilibrium and Applications is a computer code developed by NASA Lewis Research Center that encloses more than forty years of research effort in methods for the determination of complex chemical equilibrium. This main goal has been extended in order to calculate some thermodynamic properties of equilibrium mixtures. These results were applied to the resolution of common engineering problems as:

- Obtaining chemical composition and related mixture properties for a given thermodynamic state, which can be specified by assigning two thermodynamic state function. This feature is useful to get different engineering charts like the Mollier diagram;

- Calculating theoretical rocket performance;

- Calculating Chapman-Jouguet detonations;

- Calculating shock tube parameters.

The second feature of the above list is defined as the *rocket problem* in CEA.

Inputs required by the *rocket problem* are: propellant formulation, combustion chamber pressure, supersonic area ratio and combustion chamber to

throat area ratio. The latter is needed only if the finite area combustion chamber option is chosen, but in preliminary analysis this generally doesn't occur. With the given inputs an iterative procedure is applied in order to get the temperature to which the gases enthalpy value matches the reactant enthalpy. Here the adiabatic combustion chamber hypothesis is used. At that temperature and pressure corresponds a propellant gasses chemical formulation obtained using the free-energy minimization method[1]. The output obtained by now are related to the infinite area combustion chamber. If the flow is considered chemically frozen then the chemical composition will remain the same through the nozzle. With CEA it's possible to consider a chemical equilibrium flow. Hence equilibrium temperature and chemical composition are calculated at the throat and exit sections. Propellant characteristic velocity $(c^\star)$ is then calculated along with the nozzle thrust coefficient (c_F) in order to get the motor vacuum specific impulse $(I_{sp,vac})$.

The I_{sp} information is useful to understand the propulsive system theoretical performance, and the optimal working range. For the ablation modelling purpose the most interesting outputs are combustion chamber temperature and chemical composition.

In some operating conditions a condensed phase could be present according with equilibrium calculation, if the relative molar fraction is too high CEA could stop and print an error message. In this case the *omit* option could be used in order to exclude the specific chemical species.

Even if a GUI[2] for CEA is available the computer program can be executed with the following procedure:

- Creation of file `example.inp` containing the required problem, input and options in the proper format;

- Execution of `FCEA2.exe`;

- File `example.out` readout.

The next section will explain how this procedure is run automatically.

2.2 CEA BASED LOOK-UP TABLE GENERATION

NASA's CEA is a useful computer program for an engineer but the outputs are not immediately usable since they are contained in a printout as `example.out`. So to use them in a self-developed code an I/O interface code was developed in *MATLAB*®.

---

[1] The chemical composition was anyway obtained during the previous iterative procedure in order to calculate the mixture enthalpy.
[2] Graphical User Interface

The code requires the specification of oxidizer and fuel, they can be present in `thermo.inp` database or introduced in the code by the user along with their enthalpies of formation, effective oxidizer to fuel ratio (o/f), combustion chamber pressure (p_{cc}) and geometric parameter. These inputs are then printed in a file with `.inp` extension in format readable by `FCEA2.exe`. During this process the chemically frozen flow option is used. The CEA computer program is then run and the `.inp` file is specified as the file containing the program inputs. After CEA finishes its calculation, it generates a file with the same name as the input file but with the `.out` extension. The rows of this printout are then transformed into line of a matlab cell array and the extraction of the useful data takes place.

After the output relative to the frozen flow are memorized the same process takes place using the equilibrium flow option.

The code as presented by now could be introduced in another script where thermochemical data are required but this could increase the overall computational time. When this happens it is common practice to create a look-up table.

A look-up table is a matrix where the row and column numbers are related to two variables, here p_{cc} and o/f, and the element identified by these numbers is the dependent variable. This system characterizes a function of two variables.

The number of tables needed are equal to the number of properties of interest. Then required thermochemical properties are obtained by numerical interpolation of the values reported in the look-up table.

The species molar fraction look-up table is a three dimensional matrix, where the third index is related to the chemical species name. Since the number of present species changes with the propellant formulation a procedure to maintain the same order is introduced while generating the look-up table.

An example of interpolated data is shown in figure 4 where theoretical vacuum I_{sp} trends are plotted. The motor operates at 69 *bar* with a supersonic area ratio (ε) of 10, the fuel is paraffin. These operating condition were chosen to make a comparison with the figure at page 582 of reference [4].

2.3 THERMODYNAMIC AND TRANSPORT PROPERTIES

In normal operating conditions the propellant gasses can be considered made of H_2O, CO_2, CO, N_2, O_2, OH, O and NO, which are present in major quantity. For these species the investigation of thermodynamic and transport is required since they are further needed.
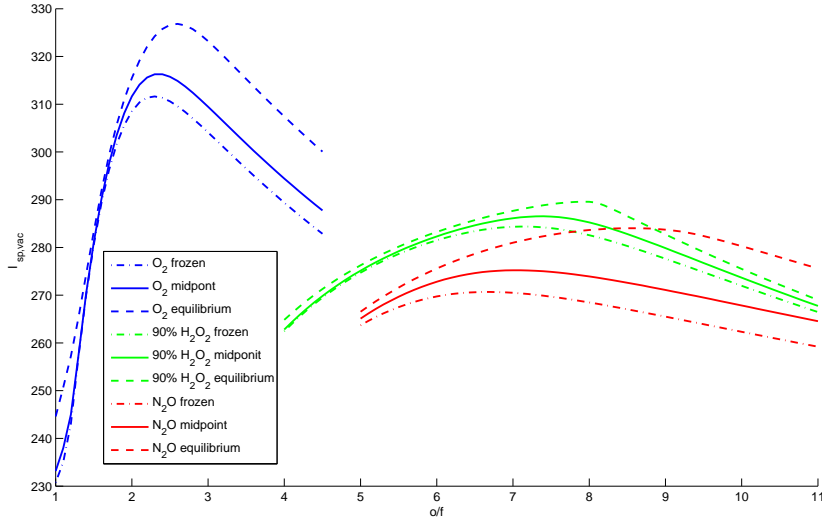
Figure 4: Vacuum I_{sp} trend obtained with CEA

Even if CEA gives the propellant specific heat (c_p) as a output, the evalua-
tion of this property for every single species is made. The species heat capacity
$(c_{p,i})$ is obtained using *Chase M.W. Jr.* interpolating function described in [5]:

$$c_{p,i} = A + B \cdot t + C \cdot t^2 + D \cdot t^3 + E/t^2 \qquad \text{where} \quad t = T/1000$$

Hence species enthalpy can be directly computed:

$$H_i - \Delta_f H_i = A \cdot t + B \cdot t^2/2 + C \cdot t^3/3 + D \cdot t^4/4 - E/t + F$$

Propellant heat capacity (c_p) is then obtained:

$$c_p = \sum_i Y_i \, c_{p,i}$$

where Y_i are species mass fractions.

Other required gas transport properties are viscosity and thermal conduc-
tivity. To obtain a viscosity function of temperature the *Sutherland equation*
was used.

$$\mu_i = \mu_{0,i} \frac{T_{0,i} + C_i}{T + C_i} \left(\frac{T}{T_{0,i}} \right)^{\frac{3}{2}} \tag{1}$$

Even if some *Sutherland* species coefficients (C_i), with the relative reference
temperature $(T_{0,i})$, were present in few databases, it was chosen to compute
them from two viscosity values, obtained from NIST[3] reference database [6],

---

3 National Institute of Standard and Technology

that better suited the operative temperature range. Data relative to H, OH and NO were unavailable and so constant values based on kinetic gas theory were adopted.

The propellant viscosity was computed using the *Wilke mixing law*:

$$\mu = \sum_i \frac{X_i \mu_i}{X_i + \sum\limits_{j;j\neq i} X_j \Phi_{ij}}$$

where X_i are species molar fractions and Φ_{ij} are viscosity interaction coefficients, which most common form is:

$$\Phi_{ij} = \frac{1}{4} \left[1 + \left(\frac{\mu_i}{\mu_j}\right)^{\frac{1}{2}} \left(\frac{M_j}{M_i}\right)^{\frac{1}{4}} \right]^2 \left(\frac{2M_j}{M_i + M_j}\right)^{\frac{1}{2}} \tag{2}$$

where M_i and M_j are molecular weights of species i and j.

Regarding the thermal conductivity individual functions of the temperature were obtained by data fitting. These functions were third or fifth order polynomials when data were available in NIST reference database [6], otherwise constant values were used.

Then propellant thermal conductivities were calculated using the following mixing law:

$$\lambda = \sum_i \frac{X_i \lambda_i}{X_i + \sum\limits_{j;j\neq i} X_j \psi_{ij}}$$

where ψ_{ij} is the following interaction coefficient:

$$\psi_{ij} = \Phi_{ij} \left[1 + \frac{2.41 \left(M_i - M_j\right)\left(M_i - 0.142 M_j\right)}{\left(M_i + M_j\right)^2} \right]$$

here Φ_{ij} is the viscosity interaction coefficient in equation 2.

These thermodynamic and transport properties will be used further in this work.

3

CONVECTIVE HEAT TRANSFER EVALUATION

Nozzle wall heat flux is the reason why thermal protection systems are needed, in fact it can reach levels of MW/m^2. In the throat region they reach the highest value. In the most general scenario they are composed by a convective component and a radiative one.

The radiative component is the sum of the flux from the hot gas and the energy re-radiated back from the wall. In HRM the exhaust gas emissivity could vary significantly. As explained in chapter 1 one way to increase HRM regression rate and adiabatic flame temperature is to introduce metallic particles into the fuel grain. This method increases the average gas emissivity in order to raise the radiative heat flux from the flame to the fuel grain. A little side effect is that this increases also the heat transferred to the nozzle. Another consideration to be done is that treating with a gaseous emitter could be not as simple as a solid one. Since the thermal protection emissivity is quite high and constant the re-irradiated heat flux depends more from the nozzle geometry and wall temperature trend.

Even if gas emissivity is high, the relative radiative heat flux is generally small compared to the convective heat, at least in the nozzle hence it can be neglected.

Since an evaluation of overall radiative heat flux is not straightforward[1] and it's contribution is only a fraction of the convective heat flux, its evaluation is generally considered an advanced step in nozzle design. Hence in this thesis the only convective heat flux is evaluated.

There are many way to estimate the convective heat flux transferred from the flow to the nozzle wall.

The first method introduced in order to avoid an expensive trial and error procedure was the *Reynolds analogy*, this permitted to get the film coefficient by the evaluation of the wall friction coefficient. This method was refined to get a better estimate using direct experimental data and shifting the trend obtained with the *Reynolds analogy*, an example of such method is the intensively used *Bartz equation*.

With the coming of CFD computer programs a different approach could be used to obtain the desired evaluation. This more general and precise way was and currently is computationally slower than the *Reynolds analogy*.

In this thesis work both approaches were used and a comparison between them is presented further.

---

1 It require advanced methods and knowledge of nozzle wall temperature along the contour.

Another important point that could make the difference from the two methods, other than precision and general application is the estimate of the diffusion coefficient (diffusivity).

Diffusivity is a key feature in thermal protection design since it limits the amount of chemical species that reach the surface to react with the thermal protection material.

With CFD the diffusivity can be simultaneously computed and the related effects can be taken into account. With traditional methods, which consist to apply another *Reynolds analogy* for close to unity *Lewis numbers*, this step takes place after the convective heat transfer evaluation an so any effect related to the diffusion and the surface erosion must be considered after using an iterative procedure.

3.1 REYNOLDS ANALOGY

With *Reynold analogy* it is possible to obtain useful information on the convective heat transfer from turbulent boundary layer similarities. Indeed, under particular hypotheses the temperature profile is quite similar to the velocity profile through the boundary layer, and since the wall convective heat flux is $q_w = \lambda \frac{\partial T}{\partial y}\big|_w$ (with λ gas thermal conductivity) it is needed to get the temperature profile in order to obtain the heat flux.
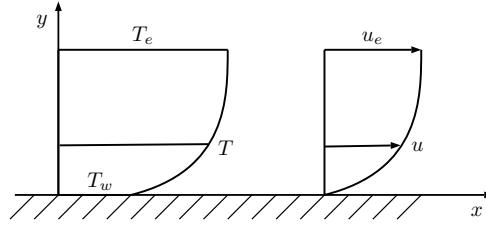
Figure 5: Temperature and velocity similarity through the boundary layer, $_e$ and $_w$ subsctipts refer to free stream and wall conditions respectively

Referring to figure 5 the boundary layer governing equations are:

$$\text{X momentum} \qquad \rho u \frac{\partial u}{\partial x} + \rho v \frac{\partial u}{\partial y} + \frac{\partial p}{\partial x} = \frac{\partial \tau_{xy}}{\partial y} \tag{3}$$

$$\text{Y momentum} \qquad \frac{\partial p}{\partial y} = 0$$

$$\text{Energy equation} \qquad \rho u \frac{\partial h^\circ}{\partial x} + \rho v \frac{\partial h^\circ}{\partial y} = \frac{\partial}{\partial y}\left(u \tau_{xy}\right) + \frac{\partial}{\partial y}\left(\lambda \frac{\partial T}{\partial y}\right) \tag{4}$$

here:

- $\tau_{xy} = \mu \frac{\partial u}{\partial y}$ is the shear stress on the face normal to y through x, i.e. friction.

- λ and μ are propellant thermal conductivity and viscosity already discussed in chapter 2;

- $h^\circ = h + \frac{u^2}{2}$ is the total enthalpy;

- u e v are components of the velocity along axis x e y respectively.

The right hand side of equation 4 can be rearranged as:

$$
\begin{aligned}
\frac{\partial}{\partial y}\left(u\tau_{xy}\right) + \frac{\partial}{\partial y}\left(\lambda \frac{\partial T}{\partial y}\right) &= \frac{\partial}{\partial y}\left(u\mu \frac{\partial u}{\partial y}\right) + \frac{\partial}{\partial y}\left(\lambda \frac{\partial T}{\partial y}\right) \qquad (5) \\
&= \frac{\partial}{\partial y}\left(\mu\left(u\frac{\partial u}{\partial y} + \frac{K}{\mu}\frac{\partial T}{\partial y}\right)\right) \\
\text{perfect gas hypothesis} \quad &= \frac{\partial}{\partial y}\left(\mu\left(u\frac{\partial u}{\partial y} + \frac{\lambda}{\mu c_p}\frac{\partial h}{\partial y}\right)\right) \\
\text{since } Pr = \frac{\mu c_p}{\lambda} \quad &= \frac{\partial}{\partial y}\left(\mu\left(\frac{\partial \frac{1}{2}u^2}{\partial y} + \frac{1}{Pr}\frac{\partial h}{\partial y}\right)\right)
\end{aligned}
$$

In rocket motor nozzle it is allowed to assume that the *Prandtl number* is close to unity, since the flow is turbulent and that is approximatively the magnitude.

Under the following hypothesis:

- $Pr = 1$, which is a good match for turbulent flows;

- $\frac{\partial p}{\partial x} \approx 0$, which is verified in the nozzle throat region;

equations 3 and 4 become:

$$
\rho u \frac{\partial u}{\partial x} + \rho v \frac{\partial u}{\partial y} = \frac{\partial}{\partial y}\left(\mu \frac{\partial u}{\partial y}\right)
$$

$$
\rho u \frac{\partial h^\circ}{\partial x} + \rho v \frac{\partial h^\circ}{\partial y} = \frac{\partial}{\partial y}\left(\mu \frac{\partial h^\circ}{\partial y}\right)
$$

which are the same differential equation.

Since the variable h° and u have different boundary condition[2], they can be transformed into h' e u' defined as follow:

$$
u' = \frac{u}{u_e} \quad , \quad h' = \frac{h^\circ - h^\circ_w}{h^\circ_e - h^\circ_w}
$$

here $h'_w = u'_w = 0$, $h'_e = u'_e = 1$ and since they are variables of the same equation with the same boundary condition:

$$
\frac{u}{u_e} = \frac{h^\circ - h^\circ_w}{h^\circ_e - h^\circ_w} \xRightarrow{u_w = 0} \frac{u}{u_e} = \frac{h^\circ - h_w}{h^\circ_e - h_w} \qquad (6)
$$

---

2 Boundary conditions are considered at the wall and free stream.

This equation is an analogy between velocity u and total enthalpy h° and it is a key feature to understand the *Reynolds analogy* between shear stress and convective heat.

Since the convective heat transfer is:

$$
\begin{aligned}
q_w &= \left. \lambda \frac{\partial T}{\partial y} \right|_w = \left. \frac{K}{c_p} \frac{\partial h}{\partial y} \right|_w \overset{u_w=0}{=} \left. \frac{\lambda}{c_p \mu} \mu \frac{\partial h^\circ}{\partial y} \right|_w \\
&= \left. \frac{1}{Pr} \mu \frac{\partial h^\circ}{\partial y} \right|_w \overset{Pr \approx 1}{=} \left. \mu \frac{\partial h^\circ}{\partial y} \right|_w \\
\text{equation } 6 \quad &= \left. \mu \frac{\partial}{\partial y} \left(h_w + (h_e^\circ - h_w) \frac{u}{u_e} \right) \right|_w = \left. \frac{h_e^\circ - h_w}{u_e} \mu \frac{\partial u}{\partial y} \right|_w
\end{aligned}
$$

(7)

And since $\tau = \mu \frac{\partial u}{\partial y}$:

$$
q_w = \frac{h_e^\circ - h_w}{u_e} \tau_w
$$

(8)

The latter equation is the *Reynolds analogy* between wall shear stress and convective heat transfer. This is a useful method to get information about heat transferred by convection to the wall from the hot gas flow from an estimate of the wall shear stress. It turns particularly valuable in understanding which trend the flux will follow varying the parameters that govern the phenomena. It is needed to remember that the hypotheses underlying the analogy are good only in the throat region and so an extension on the other nozzle zone would not be rigorous. Anyway the throat is a nozzle region of interest since here the convective heat fluxes reach the highest values.

The wall shear stress can be computed using the *dimensional analysis* equation:

$$
\tau_w = \frac{1}{2} C_F \rho_e u_e^2
$$

here C_F is the friction coefficient and can be estimated in several ways.

Introducing the above into equation 8:

$$
q_w = \frac{h^\circ - h_w}{u_e} \frac{C_F}{2} \rho_e u_e^2
$$

$$
\begin{aligned}
q_w &= \frac{h^\circ - h_w}{u_e} \frac{C_F}{2} \rho_e u_e^2 \\
&= \frac{C_F}{2} \rho_e u_e (h^\circ - h_w)
\end{aligned}
$$

(9)

If the gas is considered ideal:

$$
q_w = \frac{C_F}{2} c_p \rho_e u_e (T^\circ - T_w)
$$

Hence the convective heat transfer coefficient is:

$$\alpha = \frac{C_F}{2} c_p \rho_e u_e$$

Since the *dimensional analysis* for the convective heat transfer produced the following equation:

$$\alpha = C_H \rho_e u_e c_p$$

another common way to express the *Reynolds analysis* is:

$$C_H = \frac{C_f}{2}$$

were C_H is the *Stenton number*.

Traditionally, methods to estimate the friction coefficient were based on fully developed turbulent boundary layers in pipes friction evaluation. In [8] the *Blasius equation* is proposed:

$$C_f = \frac{0.0256}{R_e^{0.25}}$$

Another possible equation presented in [9] can be:

$$C_f = \frac{0.048}{R_e^{0.2}}$$

where *Re* is the *Reynolds number*:

$$Re = \frac{\rho_e u_e D}{\mu_e}$$

with:

- D is the hydraulic diameter;

- ρ_e free stream density;

- μ_e free stream viscosity.

So to summarize, under the hypotheses that $Pr = 1$ and $\frac{\partial p}{\partial x} = 0$ the heat flux is proportional to $\frac{C_F}{2} c_p \rho_e u_e$ and the driving force $(T^\circ - T_w)$.

But what if the *Prandtl number* is slightly different from unity and $\frac{\partial p}{\partial x} \neq 0$? In [8], Bartz presents a method to predict heat fluxes bypassing these hypotheses.

3.1.1 *Prandtl-number correction to the Reynolds analogy*

If $Pr \neq 1$ then a correction to the *Reynolds analogy* must be applied in order to better predict the convective heat flux behaviour. Different corrections established by experimental correlation are possible.

A first correction involves the convective heat driving force $(T° - T_w)$ previously introduced. It was found that a more appropriate way to express the potential was to replace the total temperature $T°$ or enthalpy $h°$ with the adiabatic wall temperature $T_a w$ or enthalpy $h_a w$, which is the temperature that the wall would reach if it didn't convey the heat elsewhere.

A way to express the adiabatic wall condition is using the *recovery factor*:

$$R = \frac{h_{aw} - h_e}{h° - h_e} = \frac{T_{aw} - T_e}{T° - T_e}$$

hence:

$$h_{aw} = h_e + R\left(h° - h_e\right) = h_e + R\frac{u_e^2}{2}$$

$$T_{aw} = T_e + R\left(T° - T_e\right) = T_e + R\frac{u_e^2}{2 \cdot c_p}$$

From the theory the following relation has been shown to be a good way to estimate the recovery factor:

$$R = Pr^{\frac{1}{3}}$$

Another Prandtl-number correction of the *Reynolds analogy* consists in the relation between *Stenton number* and *friction coefficient*. A widely valid and probably the more appropriate of these corrections was presented by *von Kármán*:

$$C_H = \frac{C_f/2}{1 - 5\left(\frac{C_f}{2}\right)^{\frac{1}{2}}\left[1 - Pr + \ln\left(\frac{6}{5\,Pr+1}\right)\right]}$$

This equation was derived considering the relation between thermal resistance in laminar sub-layer and turbulent outer region.

A simpler but less widely valid correction to the *Reynolds analogy* was presented by *Colburn*:

$$C_H = \frac{C_f/2}{Pr^{\frac{2}{3}}}$$

Using the latter correction the convective heat flux becomes:

$$q_w = \frac{C_F}{2\,Pr^{\frac{2}{3}}}\rho_e u_e\left(h_{aw} - h_w\right) \approx \frac{C_F}{2\,Pr^{\frac{2}{3}}}c_p\rho_e u_e\left(T_{aw} - T_w\right)$$

3.1.2 *The Bartz Equation*

Since the previously corrections were determined with experiments in which the ratio of energy thickness to momentum thickness is constant they did not account for shape and acceleration effects. In [8], *Bartz* presents a method to do that, the result is the widely used *Bartz equation*:

$$\alpha = \frac{C}{D^{0.2}}\left(\frac{D_{th}}{R_{c,th}}\right)^{0.1}\frac{\mu_0^{0.2}\,c_p}{Pr^{0.6}}\left(\rho_e u_e\right)^{0.8}\left[\left(\frac{\rho_{ref}}{\rho_e}\right)^{0.8}\left(\frac{\mu_{ref}}{\mu_0}\right)^{0.2}\right] \tag{10}$$

here:

- C is a constant value close to 0.026;

- D_{th} is the throat diameter;

- μ_0 is the viscosity at the stagnation condition;

- u_e is the free stream velocity

The term between square brackets is often referred to as σ and is a correction factor that take into account of properties variations through the boundary layer.

$$\sigma = \left[\left(\frac{\rho_{ref}}{\rho_e} \right)^{0.8} \left(\frac{\mu_{ref}}{\mu_0} \right)^{0.2} \right]$$

here the $_{ref}$ subscript means *reference value* and it's taken for a temperature between free stream (T_e) and wall (T_w) conditions.

The quantity $(\rho_e u_e)^{0.8}$ in equation 10 can be rearranged in order to get the throat as focal point using the equivalence $(\rho_e u_e)_{th} = \frac{\dot{m}}{A_{th}} = \frac{p_{cc}}{c^\star}$ and a value of 0.026 can be used for the variable C.

$$\alpha = \left[\frac{0.026}{D_{th}^{0.2}} \left(\frac{D_{th}}{R_{c,th}} \right)^{0.1} \frac{\mu_0^{0.2} c_p}{Pr^{0.6}} \left(\frac{p_{cc}}{c^\star} \right)^{0.8} \right] \left(\frac{A_{th}}{A} \right)^{0.9} \sigma \qquad (11)$$

This equation successfully fits turbulent boundary layer calculations over the whole nozzle, some exception can be found in the entrance region where the boundary layer can be thin.
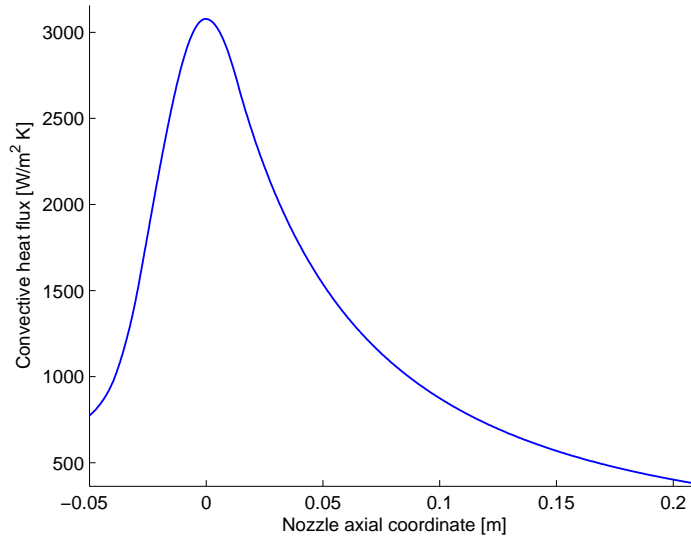

Figure 6: Film coefficient trend from equation 11

In figure 6 the film coefficient obtained in a sample case is shown. As expected the highest value is near the throat where the mass flux is higher. Farther in this chapter this trend will be compared with the one obtained via CFD computer programs.

3.2 CFD

Computational fluid dynamics computer programs are powerful tools the engineer can use to evaluate the behaviour of a fluid flow in a general system. In this thesis *ANSYS® Fluent v.14* was used on a 2D axisymmetric geometry. The system under analysis is obviously a rocket motor nozzle, in particular the BATES[3] motor nozzle geometry and operating condition were adopted.

It should be noted that for one convective heat flux characterization two CFD analyses are required, one to predict the adiabatic wall temperature trend and the other to get the film coefficient.

```
┌──────────────┐
│   Geometry   │
└──────────────┘
       │
       ▼
┌──────────────┐   - blocking    - association
│   Meshing    │   - generation
└──────────────┘
       │
       ▼
┌──────────────┐   - material        - turbulence
│Pre-processing│     characterization   model
│              │   - boundary        - solution
└──────────────┘     conditions        initialization
       │
       ▼
┌──────────────┐   - solution monitoring
│   Solution   │   - convergence
│ calculation  │
└──────────────┘
       │
       ▼
┌──────────────┐   - results
│Post-processing│  - figures
└──────────────┘
```
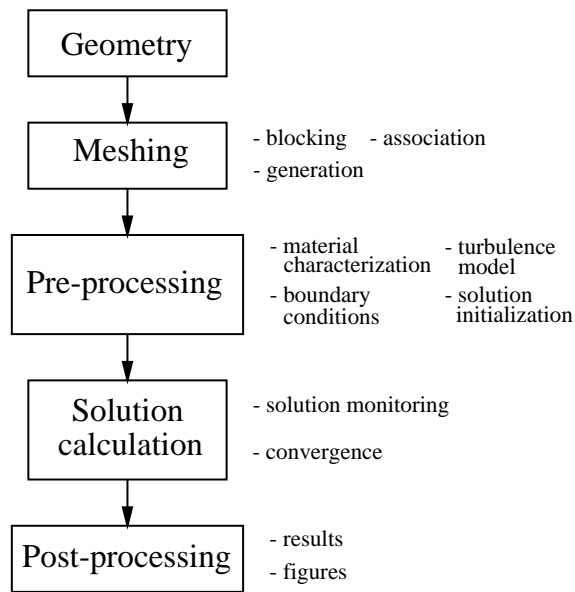
Figure 7: A general CFD procedure diagram

Figure 7 shows a general procedure used in CFD analysis. A description of how this procedure is applied to the study of a rocket motor nozzle follows.

---

3 Ballistic Test and Evaluation System

3.2.1 *Geometry*

The first step in a CFD analysis is the definition of the fluid flow domain, this is done by creating a geometry using one of the many CAD computer programs available. The important thing for the geometric model is the possibility to export it in a compatible format, such as `.igs`. This is an absolutely general way to obtain the geometry.

Since a two dimensional geometric model is not so complicated to require the use of a commercial CAD program, a different approach as been adopted. The geometry was imported directly into the meshing computer program as a file `.dat` containing the nozzle contour coordinate and general information on the geometry. This file was automatically generated using a self-developed *MATLAB®* code which required some geometric and operating parameters, the latter are needed since this code gives also some boundary conditions. The geometric parameters required can be divided in two main categories, one relative to the throat and one to the exit.
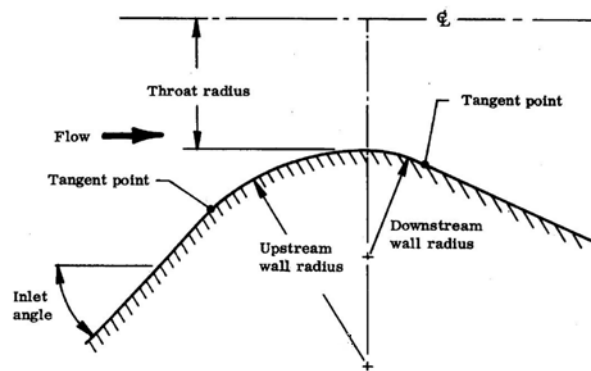
Figure 8: Nozzle throat geometric parameters [1]

In figure 8 a typical throat design is reported, it consists of an upstream circular arc tangent to a downstream circular arc at the throat location. While throat radius is imposed by motor requirements, the other geometric characteristics are based on nozzle aerodynamic design optimization or successful nozzle designs.

Geometric parameter	Range	Most near
Inlet angle	$1 \div 75°$	$45°$
Upstream wall radius	$0 \div 5 \; R_{th}$	$1 \div 2 \; R_{th}$
Downstream wall radius	$0 \div 6 \; R_{th}$	$1 \div 2 \; R_{th}$

Table 1: Successful nozzle throat parameters

The nozzle exit can be conical, or contoured, in both cases the expansion ratio (ε) is determined by nozzle performance through the operative environment, i.e. requirements, but sometimes it can be lower than the optimal value due to size and weight matters.

In conical exit nozzle a divergence half-angle between 6° to 28° has been used, most design values anyway lay in the $15 \div 17.5°$ range. Since this configuration weights a lot and has a high divergence loss factor, a contoured exit is often adopted. This allows to reduce the expansion weight maintaining the same divergence loss or vice versa. In this configuration initial divergence angles from 20° to 26° are commonly adopted. The difference between initial and final divergence normally doesn't exceeds 12°, since other losses could be introduced. Circular arcs, parabolas, splines and method of characteristics can be used then to define the nozzle contour.

In this thesis the BATES motor particular geometry was analysed. This is a conical exit nozzle and is characterized by the following parameters:

Geometric parameter	Value
Throat radius	1 *in*
Convergence half-angle	45°
Upstream wall radius	1.6 *in*
Downstream wall radius	2 *in*
Divergence half-angle	15°
Expansion ratio	10.2

Table 2: BATES nozzle geometric parameters

With the parameters reported in table 2 the *MATLAB*® program generates a file `.dat` that contains the geometry coordinate. The geometry generated by the BATES parameters is reported in figure
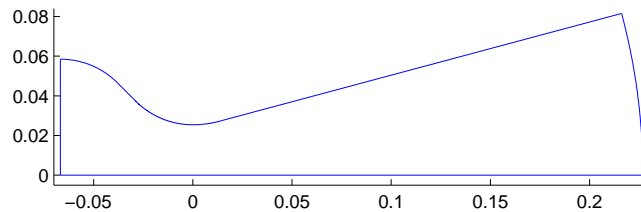

Figure 9: BATES nozzle contour generated using the MATLAB code

3.2.2 *Meshing*

The second step in a CFD analysis is the generation of a mesh, which is the division of the fluid domain into polygonal elements. In this thesis work an unstructured mesh made of quadrilateral elements was generated using *ANSYS$^{®}$ ICEM*. With this program it's possible to mesh the geometry following a *blocking strategy*. This method consists into the generation of a block (a rectangle for 2D mesh) that encompasses the initial geometry, this block can be splitted into different blocks. Their edges and vertices are then associated to geometry curves and points.

A meshing of the edges follows and this operation is extended to the block surfaces in order to obtain a division of the flow domain into quadrilateral elements. This initial mesh is refined by modifying the edge elements distribution. For example, in meshing the BATES nozzle geometry the elements size were half millimeter near the axis and one tenth of micrometer near the nozzle wall, in order to get better information in the boundary layer.

Then this pre-meshed block is converted into an unstructured mesh and saved as `.msh` format, importable in Fluent. Once it has been saved the mesh can contain information relative to the kind of boundary conditions applied at the edges.
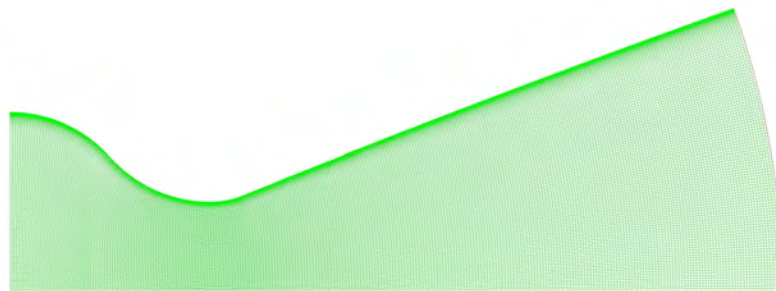
Figure 10: BATES nozzle mesh

3.2.3 *Pre-processing*

In this step the main program setup takes place. First of all the mesh previously generated must be imported, then the solution setting can take place.

In the general setup it must be specified that a steady state solution of a two-dimensional axisymmetric fluid domain is the wanted result. The type of solver is also chosen here. There are two main solver types: pressure-based and density-based. The first was historically used for incompressible fluid the second for the compressible one.

In the models setup section the physical phenomena are going to be evaluated with the analysis. Since heat transfer is considered the energy equation must be introduced in the required set of equation. Then a viscous model is chosen, here a shear stress transport k-ω turbulence model was used. Another useful model that could have been used was the species transport model in order to get a better value of the diffusivity coefficient, but this model introduces an equation per chemical species considered and then slows the solution calculation process. With the radiation model it's also possible to consider the heat transferred by radiation.

In the material setup section the fluid that composes the exhaust gasses is defined, if the species transport model was adopted then a mixture fluid model is going to be defined. Here a frozen flow of gasses produced by the reaction between paraffin and 90% pure hydrogen peroxide near the optimal o/f point was used as fluid material. The composition obtained in this conditions is reported in table 3.

Species	H_2O	CO_2	OH	O	O_2	CO	H_2	H
Mole fraction	0.753	0.141	0.02	0.001	0.02	0.04	0.032	0.003

Table 3: *WAX-* H_2O_2 typical combustion chamber composition

Using this chemical composition the gaseous mix thermochemical and transport properties functions of temperature were determined interpolating the values obtained with the procedure presented in section 2.3.

The next step on the solution setup is the definition of the boundary conditions, in this analysis they are applied to the nozzle wall, inlet and outlet. The axis condition was automatically defined, while at the wall a non-slip condition were applied for the momentum equation and a adiabatic wall or fixed temperature for the energy equation depending on the analysis purpose[4]. For the inlet a mass-flow-inlet boundary condition was used, the input mass flow has been determined using characteristic velocity correlation to the combustion chamber pressure and throat area:

$$\dot{m} = \frac{p_{cc} \, A_{th}}{c^\star}$$

while the thermal condition was the combustion chamber temperature. The outlet boundary condition was a pressure outlet but since in the divergent part of the nozzle the flow is supersonic this condition is bypassed by the solver.

---

4 If the analysis aims to determine the adiabatic wall temperature or film coefficient trend

Once the boundary conditions are defined the problem setting is complete and the solution procedure can start.

3.2.4 *Solution calculation*

First step in the solution procedure is to set the type of solver and the under-relaxation factors. During this analysis an implicit method was chosen and under-relaxation factors of 0.7 all equally set. The solution was initialized with a standard method using combustion chamber temperature and pressure as reference values. Two properties were monitored during the solution calculation other than the residuals: they were average inlet static pressure and average wall temperature or convective heat flux, as the case may be. Since the mass flow boundary condition was used, the average inlet pressure is a good property to be monitored, indeed an estimate value is available and the property convergence to that value can indicate a convergence of the free stream solution. The second parameter is used to understand if the boundary solution is converged. During the adiabatic wall temperature simulation the average temperature is monitored while the film coefficient is evaluated the average wall flux was used as reference parameter.

In evaluating the BATES nozzle both simulation converged, and the data resulting from the adiabatic wall temperature analysis were used to initialize the film coefficient analysis solution avoiding,in this way, to increase the calculation time.

3.2.5 *Post-processing*

After the solution is calculated it's time for the post processing. With this step the useful results and purposes of the analyses are extracted from the intensive amount of data generated during the simulation.

From the first simulation the adiabatic wall temperature trend with the axial coordinate was obtained:

Another result obtained is the temperature profile through the boundary layer. This is not so useful itself but it shows the increase of temperature until adiabatic wall conditions are reached. This is the main difference from the most used low-speed approximation where static temperature is used as driving force.

Fluent also allows to export figures, they can be used to see if something bizarre happens in the fluid flow and to understand if the solution effectively converged.

In figure 13 the following effects can be observed:

- The wall is lined by a red line meaning the increase of temperature to the adiabatic wall condition close to the stagnation one;
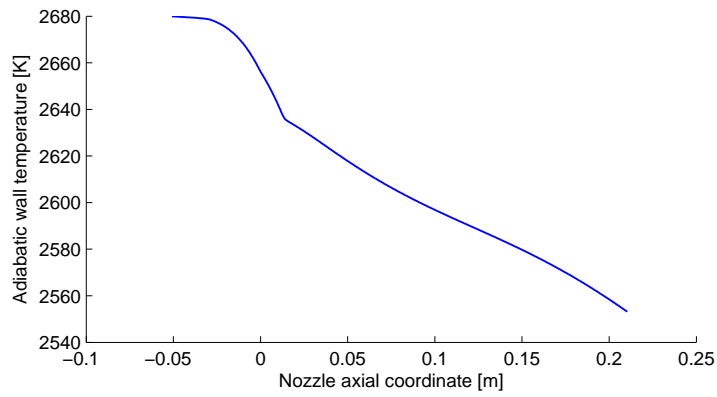
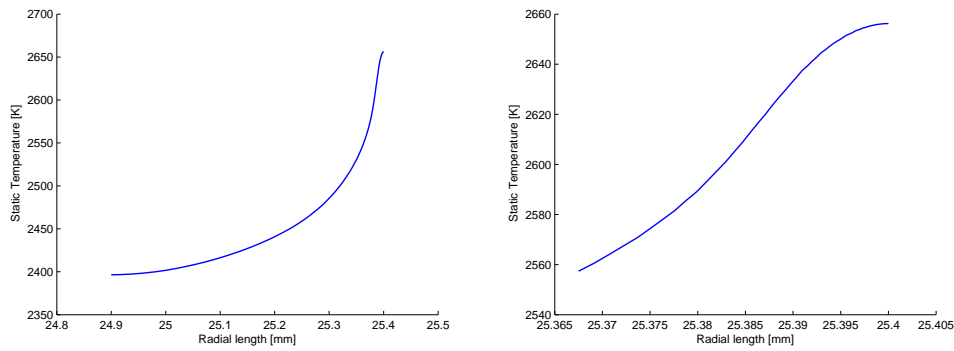Figure 11: Adiabatic wall temperature trend from the CFD analysis

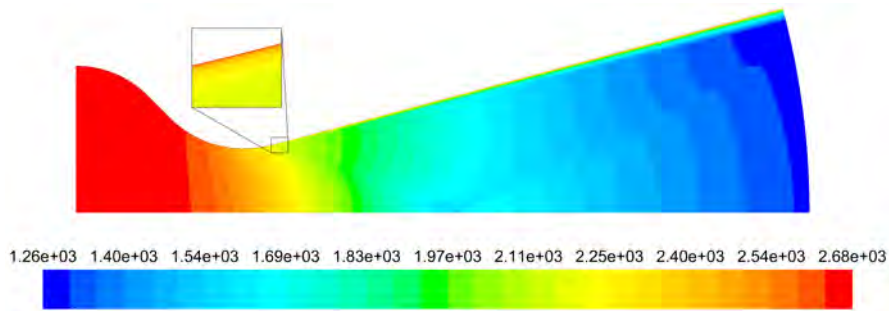Figure 12: Temperature rising through the boundary layer

Figure 13: Static temperature in BATES nozzle from the CFD analysis

- Short after the throat region an oblique line, at which a discontinuity takes place, can be detected, this is an oblique shock effect;

28

- At the wall point where the shock starts, corresponds the step change of slope in figure 11.

The second analysis was used instead to obtain the convective heat transfer coefficient trend:
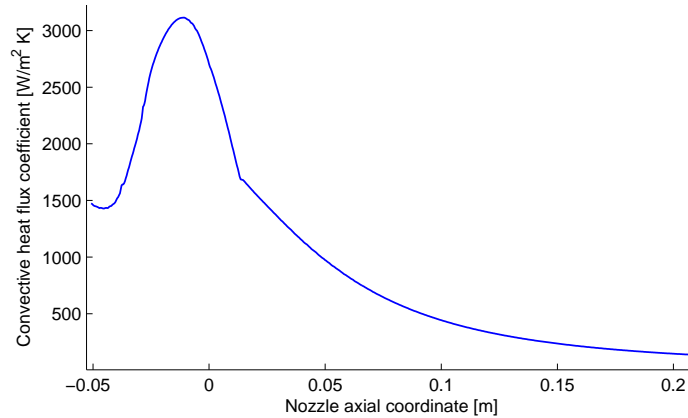
Figure 14: BATES nozzle film coefficient trend from CFD analysis

With the film coefficient a similar step change in the slope to the one in figure 11 (adiabatic wall temperature) can be noted at the same nozzle axial coordinate.

3.3 COMPARISON

Since two are the methods to predict the convective heat presented before a comparison between them is presented in this section.

Let's discuss the driving force differences first. In figure 15 a comparison of three ways to get the adiabatic wall temperature is showed. The classic *Prandtl number correction* (blue line) which consists in using a recovery factor of $Pr^{\frac{1}{3}}$ gives too high adiabatic wall temperature. This turns into a higher erosion rate, that could not be a problem during the design phase but could be undesired in preliminary performance evaluation. Anyway a difference of 20 *K* at the throat can be insignificant.

The CFD solution (red line) shows a similar behaviour in the convergent and throat region to the one obtained with the use of recovery factor, but then a change happens short after the throat.

The black line shows the trend obtained with a less classic method. This consists in the use of a recovery factor equal to 0.9 regardless of the effective *Prandtl number*. Here this solution sticks to the one obtained from CFD until the step change of the latter.
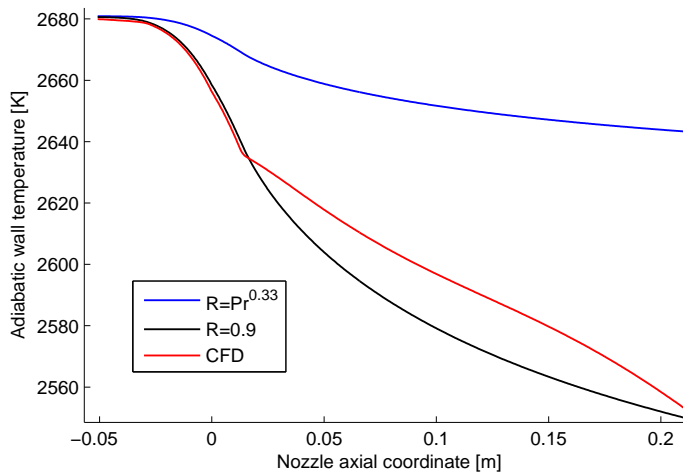
Figure 15: Adiabatic wall trends temperature comparison

Method	at the throat	max difference
$R = Pr^{1/3}$	19.0 K	90.2 K
$R = 0.9$	2.3 K	−17.9 K

Table 4: Adiabatic wall temperature methods comparison

In table 4 the numerical differences between the recovery factor methods and the results obtained with the CFD analysis are reported. With the classic method $\left(R = Pr^{1/3}\right)$ temperature differences up to 90 K are reached while at the throat the spread is reduced to 19 K. These values are high but not so critical in the design phase since:

- At the throat the difference is quite low and could be a problem only for very high wall temperatures;

- In the diverging section where the estimated adiabatic temperature difference is high the wall temperature is generally low and hence low is the related error;

- The estimate is always higher then the CFD one and this can only leads to a over-predicted design which is not usually a problem.

By imposing $R = 0.9$ the adiabatic wall temperature results more accurate than the one obtained with the previous method but in the divergent section the spread becomes negative, and this can lead to under predict the required insulator thickness.

Figure 16 shows the differences in the methods used to estimate the convective heat coefficient:
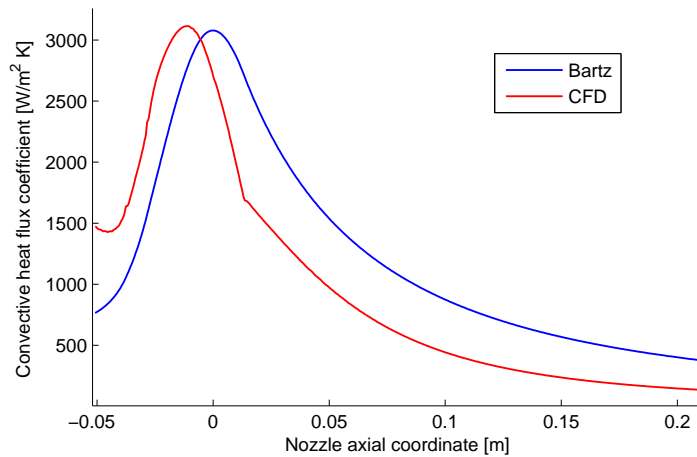
Figure 16: Convective heat transfer coefficient trends comparison

- The *Bartz equation* maximum occurs at the throat, while the CFD analysis shows that the maximum occurs upstream of the nozzle throat. The relative difference between the peaks is 1.2%, while at the throat ($x = 0$) the spread is about 15.6%, with respect to the CFD maximum;

- The Bartz method over-predicts the film coefficient in the divergent section, and it's about 1.7 times greater than the CFD calculation;

- Approaching the convergent section, the CFD solution shows higher values than the *Bartz* solution due to boundary layer growth.

Results found during this comparison are analogous to those reported in [10], figure 17 here. The CFD trend has to be considered more accurate than the one obtained using *Bartz equation* and *Prandtl number correction* but, on the other hand, these methods require less computational time than a CFD analysis. So during a preliminary design procedure the much faster and slightly less precise method can be used, in particular at the throat where the relative difference between the methods is quite low.

3.4 BLOWING RATE CORRECTION

Mass injection in the boundary layer can reduce the convective heat transfer, this is known as *blowing effect*. This phenomena occurs in ablative thermal protections and it's a benign effect since it reduces the incoming heat. This effect is commonly accounted using the following *Stenton number* correction:

$$C_H = C_{H_1} \frac{\zeta}{e^\zeta - 1}$$
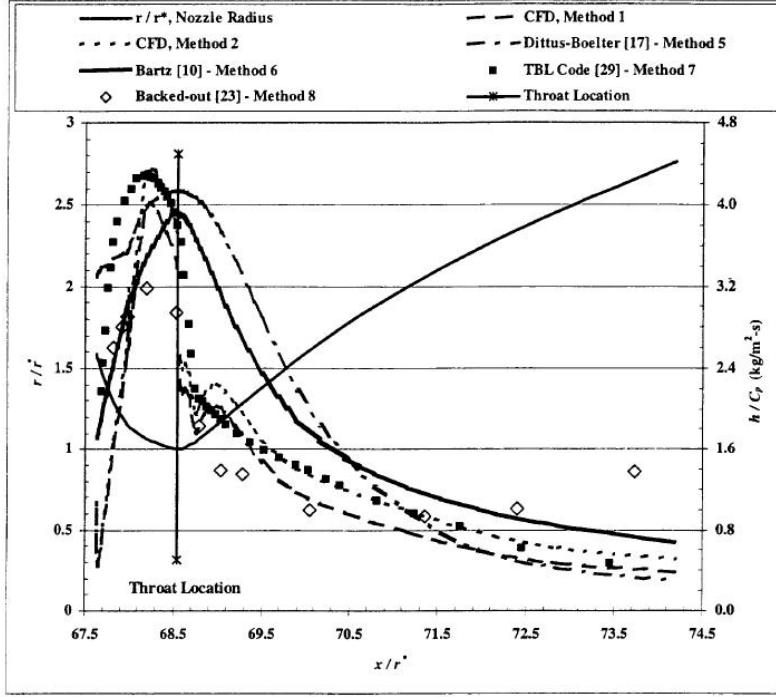
Figure 17: Different methods convective heat transfer coefficient trends comparison, from reference [10]

where:

$$\zeta = \frac{2 \lambda \dot{m}}{\rho_e \, u_e \, C_{H_1}}$$

here:

- λ is the blowing rate parameter;

- $\dot{m}$ is the gaseous mass being injected into the boundary layer;

- $\rho_e \, u_e \, C_{H_1}$ is the non-blowing heat transfer coefficient.

The blowing rate parameter (λ) can assume different values. The value $\lambda = 0.5$ lead to the classical blowing correction which agree with most experimental results:

$$\frac{C_H}{C_{H_1}} = \frac{ln \left(1 + \dot{m}/\rho_e \, u_e \, C_{H_1}\right)}{\dot{m}/\rho_e \, u_e \, C_{H_1}}$$

It must be noted that $\dot{m}$ is only the gaseous mass injected into the boundary layer, so any mechanical failure or liquid removal from the surface doesn't contribute to the convective heat flux reduction and hence they reduce the effectiveness of the thermal protection.

The study of chemical species diffusion through the boundary layer is a main matter in thermochemical erosion evaluation since diffusion regulates the amount of gaseous reactants that reach the solid thermal protection. Even if this topic seems unrelated with the convective heat transfer analysis it was introduced here for reasons that will be further revealed.

There are many way to model the mass diffusion flux, one of this is the *Fick's law*:

$$\dot{m}_{diff} = \rho \, D_i \, \nabla Y_i$$

where D_i is the species diffusion coefficient. The previous equation become at the wall:

$$\dot{m}_{diff} = \rho D_i \frac{\partial Y_i}{\partial y}\bigg|_w$$

If the equal diffusion coefficients hypothesis is used, then the species diffusion become:

$$\dot{m}_{diff} = \rho D \frac{\partial Y_i}{\partial y}\bigg|_w$$

Unfortunately the determination of the diffusion coefficient (D) is not immediate, it requires the use of an analogy between chemical concentration and total enthalpy profiles through the boundary layer, in order to estimate the species mass flux transmitted.

In section 3.1 the following equation was deduced:

$$q_w = \lambda \frac{\partial T}{\partial y}\bigg|_w = \frac{\lambda}{c_p} \frac{\partial h}{\partial y}\bigg|_w \overset{u_w=0}{=} \frac{\lambda}{c_p} \frac{\partial h^\circ}{\partial y}\bigg|_w$$

Dividing then q_w by $\dot{m}_{diff}$ the following relation is obtained:

$$\frac{q_w}{\dot{m}_{diff}} = \frac{\rho D c_p}{\lambda} \frac{\partial Y_i}{\partial y} \frac{\partial y}{\partial h^\circ}\bigg|_w = \frac{\rho D c_p}{\lambda} \frac{\partial Y_i}{\partial h^\circ}\bigg|_w \tag{12}$$

Under appropriate hypotheses, equation 12 drives to the *Reynolds analogy* between the convective heat transfer and the species mass diffusivity at the wall. The appropriate hypotheses are the following:

- Close to unity *Lewis number*, $(Le \approx 1)$;

- Similitude between the species concentration and the total enthalpy profiles through the boundary layer.

The first hypothesis is a direct result of other two numbers being close to unity. These are the already cited *Prandtl number* and the *Schmidt number*:

$$Pr = \frac{\mu c_p}{\lambda} \approx 1 \quad , \quad Sc = \frac{\mu}{\rho D} \approx 1$$

And hence the *Lewis number*, which correlate the diffusivity phenomena with the convective heat flux is close to unity too.

$$Le = \frac{Sc}{Pr} = \frac{\mu}{\rho D} \frac{\lambda}{\mu c_p} = \frac{\lambda}{\rho D c_p} \approx 1$$

The *Lewis number* is also the reciprocal of the proportionality constant in equation 12, which becomes:

$$\frac{q_w}{\dot{m}_{diff}} = \frac{1}{Le} \left.\frac{\partial Y_i}{\partial h^\circ}\right|_w \approx \left.\frac{\partial Y_i}{\partial h^\circ}\right|_w$$

The similarity between the species concentration and the total enthalpy through the boundary layer involves the following identity:

$$\frac{Y - Y_w}{Y_e - Y_w} = \frac{h^\circ - h^\circ_w}{h^\circ_e - h^\circ_w}$$

and hence:

$$Y = Y_w + \frac{Y_e - Y_w}{h^\circ_e - h^\circ_w} (h^\circ - h^\circ_w)$$

This implies that the derivative of Y with respect to h° is:

$$\frac{\partial Y}{\partial h^\circ} = \frac{Y_e - Y_w}{h^\circ_e - h^\circ_w}$$

And hence equation 12 becomes:

$$\frac{q_w}{\dot{m}_{diff}} = \frac{1}{Le} \left.\frac{Y_e - Y_w}{h^\circ_e - h^\circ_w}\right|_w \approx \left.\frac{Y_e - Y_w}{h^\circ_e - h^\circ_w}\right|_w$$

The diffusive mass flux can then be determined using the following analogy:

$$\dot{m}_{diff} = \rho D \frac{\partial Y_i}{\partial y} = \frac{Y_e - Y_w}{h^\circ_e - h^\circ_w} q_w \tag{13}$$

Introducing the calorically perfect gas hypothesis and the convecting heat definition previously achieved the analogy in equation 13 becomes:

$$\rho D \frac{\partial Y_i}{\partial y} = \frac{\alpha}{c_{p_{prop}}} \frac{T_{aw} - T_w}{T^\circ_e - T_w} (Y_e - Y_w) \tag{14}$$

The analogy obtained undergoes a series of more or less strong hypotheses, but still allows to estimate properly the diffusive mass flux. If more accuracy is required the following general equation can be used:

$$\dot{m}_{diff} = \rho_e \, u_e \, C_M \, (Y_e - Y_w)$$

where C_M is mass transfer coefficient and is related to the *Stanton Number* (C_H) using the *Chilton-Colburn relation*:

$$C_M = Le^{\frac{2}{3}} C_H$$

ABLATION PHYSICS AND MODELLING

In previous chapters, important aspects regarding the hybrid rocket motor thermochemical environment were presented regardless of the system used to protect the nozzle. In this chapter a method that allows the nozzle to safely operate under the harsh environment and trough all the component operating time, is presented, along with the model implemented in a *MATLAB®* code to simulate the erosion mechanism behaviour.

Then the code will be applied to the BATES motor study case, presented in the reference paper [12], in order to validate the obtained results. Once validated the code can be used to rapidly predict the erosion rate and wall temperature in the changing and peculiar thermochemical environment that characterizes a hybrid rocket engine.

Thermochemical ablation is the result of chemical reaction between gaseous chemical species in the propellant and the nozzle wall material. For a well performing ablative material it's important that the overall reaction results to be endothermic, in order to mitigate most part of the convective heat from the gas.

In chapter 1 (Introduction) two different kind of ablative thermal protection were mentioned: charring and non-charring. The difference between them lays on the in-depth thermal response and the surface thermochemical behaviour which in charring materials is altered by the pyrolysis gas presence. Hence non-charring material surface reactions result more easy to model.

4.1 ABLATION MODELS

There are different ways the ablation phenomena can be modelled. The simplest of these is the *heat of ablation model* where the erosion rate is considered proportional to the incoming heat according with the following equation:

$$\dot{e} = \frac{q_w}{\rho_c \, Q_{ab}}$$

where ρ_c is the base material or char density and Q_{ab} is the heat of ablation.

Unfortunately the heat of ablation is function of the free-stream chemical composition, other than the kind of protection material, and so this method

relies on specific experimental data, that could not be available or be extrapo-lated in the case under analysis. If a material thermochemical behaviour is too sensible to the free stream chemical composition, the nature of HRM en-vironment doesn't make the heat of ablation method suitable for the erosion estimate.

A more accurate way to predict the surface erosion is the *thermochemical ablation model* which consists in the solution of a set of equations com-posed by surface mass balances (SMB[1]s) and a surface heat balance (SHB[2]). There are two kind of thermochemical ablation models: equilibrium and non-equilibrium, depending on the chemical surface composition.

Equilibrium thermochemical ablation codes are the most diffused since they do not require information about the surface kinetics but only the surface equilibrium composition, which impose the diffusive mass fluxes driving force and the surface enthalpy to use in SMBs and SHB respectively. The most used thermochemical equilibrium ablation code is Aerotherm's EST[3], it supplies the data required for the boundary conditions calculation in the in-depth solution computer program CMA.

Non-equilibrium thermochemical ablation codes are computationally slightly more complex than the equilibrium ones, but they are not so widely used since they require accurate surface chemical kinetics data that are not so easy to get. General use thermochemical non-equilibrium ablation models are still under development but are thought to reduce the intrinsic over-design obtained with the equilibrium codes.

Both equilibrium and non-equilibrium thermochemical ablation models are normally used to get surface thermochemistry tables which allow to get the dimensionless char rate (B'_c) as a function of surface temperature, pressure and dimensionless gas rate $\left(B'_g\right)$. These dimensionless quantities are defined as follow:

$$B'_c = \frac{\dot{m}_c}{\rho_e \, u_e \, C_M} \quad , \quad B'_g = \frac{\dot{m}_g}{\rho_e \, u_e \, C_M}$$

where $\dot{m}_c$ is the char or base material mass flux and $\dot{m}_g$ is the pyrolysis gas mass flux.

In the particular case where the base material doesn't pyrolyse or de-compose the thermochemistry tables result simplified since there is one variable less. The lack of pyrolysis gasses also simplifies a thermochemical

---

1 Surface Mass Balance
2 Surface Heat Balance
3 Equilibrium Surface Thermochemistry

non-equilibrium ablation model since all the related reactions must not be taken into account.

4.2 NON-CHARRING ABLATION MODELLING

In this thesis work the non-equilibrium ablation model presented by *D. Bianchi and F. Nasuti* in [12] is used to predict the surface erosion in carbonaceous materials that do not form char: pyrolytic graphite, bulk polycrystalline graphite and carbon-carbon composites which are often used as throat insert materials.

In non-charring ablative materials erosion occur because reacting species in the free stream, that cross the boundary layer, reach the surface and react. This phenomena is described by the species surface mass balance.

4.2.1 *Surface mass balance*

Surface mass balance is the most meaningful equation of the set since it explains how the ablation dynamics occur. Let's consider a movable control volume tied to the receding surface and with small extent to the gas an solid sides as shown in figure 18.
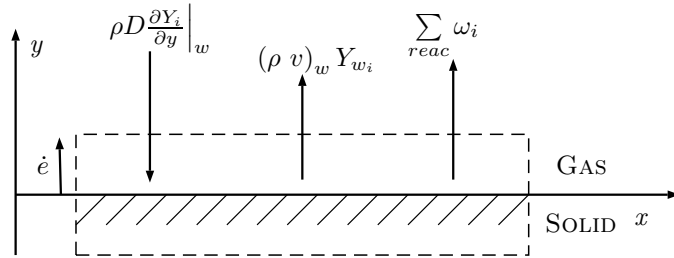
Figure 18: Species surface mass balance

The ith species mass fluxes balance in a such control volume is represented by the following equation:

$$\rho D \left.\frac{\partial Y_i}{\partial y}\right|_w = (\rho v)_w Y_{w_i} + \sum_{reac} \dot{\omega}_i \tag{15}$$

where:

- $\rho D \left.\frac{\partial Y_i}{\partial y}\right|_w$ is the species diffusive mass flux at the wall. Here it has been expressed using the *Fick's law*. In section 3.5 this quantity was rearranged as $\rho_e u_e C_M (Y_e - Y_w)$;

- $(\rho \, v)_w$ is a "blowing" term caused by the surface recession. If it's assumed that all the base material turns in gaseous reaction products, such that no mechanical erosion or surface melting occurs, this term becomes $(\rho \dot{e})$ which is also equal to the mass flux of consumed base material $(\dot{m}_c)$;

- $\sum_{reac} \dot{\omega}_i$ is the overall species reaction rate due to surface heterogeneous reaction with the ablative material. The erosion rate is directly related to these quantities via the stoichiometric coefficients and molecular weight ratios.

Hence the surface mass balance in equation 15 can be rearranged as follow:

$$\rho_e \, u_e C_M \left(Y_{e_i} - Y_{w_i} \right) = (\rho \dot{e}) \, Y_{w_i} + \sum_{reac} \dot{\omega}_i \tag{16}$$

4.2.2 Chemical reactions and kinetics

The non-equilibrium model presented in [12] consider five heterogeneous reactions to occur at the surface, these are caused by five different reacting species: H_2O, CO_2, OH, O e O_2. The relative chemical reactions are:
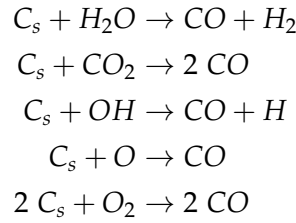
$$C_s + H_2O \rightarrow CO + H_2$$
$$C_s + CO_2 \rightarrow 2\,CO$$
$$C_s + OH \rightarrow CO + H$$
$$C_s + O \rightarrow CO$$
$$2\,C_s + O_2 \rightarrow 2\,CO$$

It's important to note that some of these reactions normally would not occur for low temperature, such as the ones that involve H_2O and CO_2, but given the high nozzle wall temperature these reactions occur and they are also important to the process since they are endothermic.

Reactant species	$\Delta H^{\circ}_{reac} \ [MJ/kg]$
H_2O	10.94
CO_2	14.37
OH	5.71
O	-29.98
O_2	-9.21

Table 5: Standard enthalpies of reaction

Table 5 shows the standard[4] enthalpies of reaction per kilo of carbon consumed. It may seem that the graphite is not a good ablative material since it involves exothermic reactions, but this is not true since there are other important parameters like: the kinetics of the reactions and exhaust composition. In solid rocket motor the high content of aluminium reduce the free oxygen content in the exhaust gas and hence increasing the related ablation effectiveness.

Figure 19 shows the extension of these enthalpies to non-standard operating conditions and a comparison between the obtained (left) and the ones reported in the reference.

(a) from calculation   (b) from paper [12]
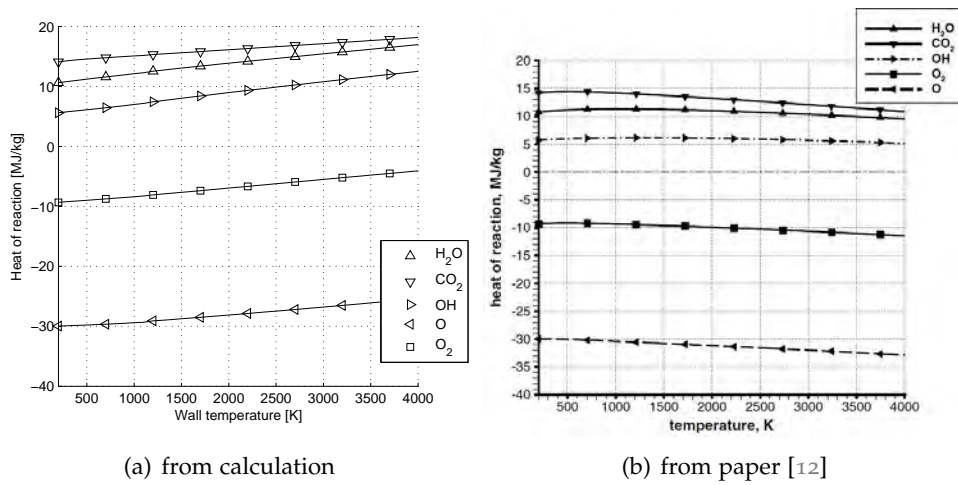
Figure 19: Heat of reactions comparison

In [12], *Arrhenius models* are used for H_2O, CO_2, OH and O reacting species, while the *Nagle & Strickland model* is used for O_2. Hence the carbon reaction rates due to the first five species are calculated with the following equation:

$$\dot{m}_i = \left(A_i T_w^{b_i} e^{\frac{-E_i}{RT_w}} \right) p_i^{n_i}$$

where:

- T_w is the adiabatic wall temperature, in this case it's the temperature at which the reactions take place;

- p_i is the ith species partial pressure, i.e. $p_i = X_i\, p$;

- A_i is the reaction pre-exponential factor;

- E_i is the reaction activation energy and R is the gas constant;

---

4 The standard reference state is the point of temperature $T = 298.15K$ and pressure $p = 1bar$.

- n_i is the pressure exponent and b_i is the temperature exponent.

For the *Nagle & Strickland model* the following equation was used instead:

$$\dot{m}_{O_2} = \frac{k_5\,p_{O_2}\,Y}{1 + K_6\,p_{O_2}} + k_7\,p_{O_2}\,(1 - Y) \quad \text{here} \quad Y = \left(1 + \frac{k_8}{k_7 p_{O_2}}\right)^{-1}$$

where k_5, k_6, k_7 and k_8 are all *Arrhenius* like rate constant.

All the required values for the described kinetic model can be found in [12] but particular attention should be given to the measurement units.

(a) from calculation   (b) from paper [12]
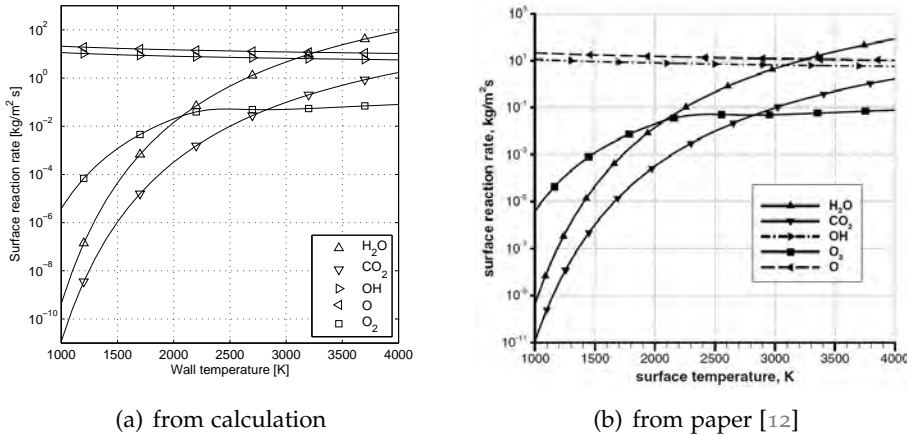
Figure 20: Surface reaction rates comparison

In figure 20, the carbon surface reaction rate caused by the reacting species is shown, a partial pressure of 1 *atm* was used. On the right the same results reported in the reference are shown. No difference can be found between the obtained and reported results.

It should be noted that the surface reaction rate is function of the wall temperature, the local static pressure and the species concentration, since the species mole fraction appears in the partial pressure term.

If no mechanical erosion or liquid phase removal occurs then the surface reaction rate is directly related to the erosion rate:

$$\dot{m}_c = \dot{m}_{H_2O} + \dot{m}_{CO_2} + \dot{m}_{OH} + \dot{m}_O + \dot{m}_{O_2} = \rho_c\,\dot{e}$$

While the species reaction rate $\dot{\omega}_i$ that appear in the SMB are obtainable using the following relation:

$$\dot{\omega}_i = \frac{M_{m,i}}{M_{m,c}}\frac{\nu_i}{\nu_c}\,\dot{m}_i$$

where $M_{m,i}$ and $M_{m,c}$ are molecular weights of the reactive species and carbon respectively, ν_i and ν_c are the relative reaction stoichiometric coefficients.

Then for given combustion chamber conditions and local static pressure, equation 16 representing the surface mass balance, results to be a function of the wall temperature and the surface chemical composition.

Hence the surface mass balance equation set of N equations, where N is the number of chemical species considered, contain $N + 1$ unknown variables: N wall species concentrations and the wall temperature. In particular the species concentrations appear in the diffusivity driving force as mass fractions and in partial pressure term in the chemical kinetics as mole fractions, while the surface temperature T_w appears mainly in the chemical kinetics related terms of species reaction rate $\dot{\omega}_i$.

The missing equation needed to get the $N + 1$ unknowns is the energy balance at the surface also known as SHB.

4.2.3 *Surface heat balance*

The surface energy balance relates the reason why thermal protections are needed with their behaviour at a given temperature, in order to find the equilibrium operating surface temperature T_w. This results to be a governing variable for the chemical kinetics which in turn affects the ablation mechanism and hence the effective heat of ablation.

Figure 21 shows the equilibrium between heat fluxes across the same movable control volume in figure 18.
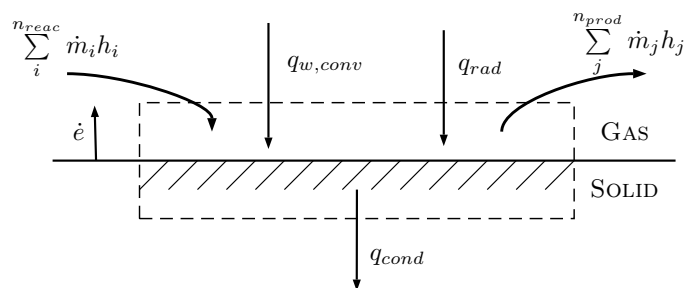

Figure 21: Graphical representation of the surface heat balance

The involved heat fluxes are:

- The wall convective heat flux $q_{w,conv}$;

- q_{rad} the overall radiative heat flux, which is the sum of heat from the semitransparent gas and the emitted flux from the nozzle wall;

- q_{cond} is the conductive heat through the base material;

- $\sum_{j}^{N_{prod}} \dot{m}_{tot,j}\, h_j - \sum_{i}^{N_{reag}} \dot{m}_{tot,i}\, h_i$ is the enthalpy difference between the gaseous products of the surface heterogeneous reactions and their reactants which are the both gasses from the free-stream and solid from the nozzle ablative material. This term is often referred to chemical heat flux q_{chem}.

The surface heat balance is then:

$$q_{w,conv} + q_{rad} = \sum_{j}^{N_{prod}} \dot{m}_{tot,j}\, h_j - \sum_{i}^{N_{reag}} \dot{m}_{tot,i}\, h_i + q_{cond} \qquad (17)$$

Convective and radiative heat fluxes have been introduced previously, in particular in chapter 3, two methods to estimate the convective heat flux were applied to a given geometry. On the other hand no method to estimate the in and out radiative flux was presented, since this procedure can be complicated, variable with the propellant formulation and can be neglected at the throat which is the region of interest in this work.

In usual procedures the conductive heat flux value is provided by an in-depth solution calculator which in turn is coupled with the ablation model. This way it's possible to take into account how transient heat conduction and storage of sensible energy phenomena influence the surface erosion rate through the nozzle operating time, in particular during the warm up. With charring ablative materials the use of this procedure is almost inevitable since other effects occur, but in this work the *heat sink* effect of the non-charring ablative materials under analysis is neglected and the steady state conductive heat flux is used.

The steady state in-depth thermal profile of a solid material with constant thermal conductivity λ, density ρ and specific heat capacity c_p is described by the following equation:

$$T = T_o + (T_w - T_o)\, e^{-\frac{\dot{e}}{\alpha} x}$$

where T_o is the initial (before ignition) temperature, x is the depth with reference to the movable coordinate system, $\dot{e}$ is the surface erosion and $\alpha = \frac{\lambda}{\rho\, c_p}$ is the thermal diffusivity. The temperature decreases exponentially with the depth, the rate of decrease is proportional to $\alpha/\dot{e}$ which is the phenomenon characteristic length. For a depth higher than three times the characteristic length the temperature deviation from the initial temperature

can be neglected. It must be noted that for high erosion rate $\alpha/\dot{e}$ is small, while for erosion rate that approaches zero the characteristic length is infinite.

The derivative of the temperature with reference to the depth is then:

$$\frac{\partial T}{\partial x} = -\frac{\dot{e}}{\alpha}\left(T_w - T_o\right)e^{-\frac{\dot{e}}{\alpha}x} \stackrel{x=0}{=} -\frac{\dot{e}}{\alpha}\left(T_w - T_o\right)$$

Hence the steady state conductive heat flux at the wall is:

$$q_{cond} = -\lambda\left.\frac{\partial T}{\partial x}\right|_w = \lambda\frac{\dot{e}}{\alpha}\left(T_w - T_o\right) = \rho\,c_p\,\dot{e}\left(T_w - T_o\right)$$

It must be noted that the quantity $\rho\,c_p\,\dot{e}\left(T_w - T_o\right)$ is the solid ablative material mass flux $\rho\,\dot{e}$ multiplied by the enthalpy change from the initial condition to the wall condition $c_p\,\left(T_w - T_o\right)$.

The last energy term in the steady state surface heat balance is the chemical heat flux q_{chem} which is the overall chemical energy difference in the control volume, this energy is known as heat of ablation since this is the heat mitigated by the ablation phenomena.

$$q_{chem} = \sum_{j}^{N_{prod}} \dot{m}_{tot,j}\,h_j - \sum_{i}^{N_{reag}} \dot{m}_{tot,i}\,h_i$$

In order to get the enthalpies differences and the related mass fluxes the chemical heat flux can be rearranged as the heat obtained from the chemical reactions that take place at the surface. Referring to the standard reference state the individual reaction heat is:

$$\sum_{prod} \dot{m}_{prod}\int_{T^{\circ}}^{T_{out}} c_p\left(T\right)dT + \Delta H^{\circ}_{reac}\dot{m}_{C,i} - \sum_{reag} \dot{m}_{reag}\int_{T^{\circ}}^{T_{in}} c_p\left(T\right)dT$$

where $T^{\circ} = 298.15$ is the standard conditions temperature, T_{in} and T_{out} are the reaction reactants and products temperatures, here both equal to the wall temperature T_w.

The reactants and products mass fluxes $\dot{m}_{reag}$ and $\dot{m}_{prod}$ are equal to the species reaction rates $\left(\dot{\omega}_i\right)$ in equation 16 and hence can be calculated using the following equation, that relates them to the ablative material reaction rates:

$$\dot{m}_i = \frac{M_{m,i}}{M_{m,c}}\frac{\nu_i}{\nu_c}\dot{m}_{c,i}$$

where M_m are molecular weights and ν are reaction stoichiometric coefficients.

The required specific heat capacity were obtained the same way described in section 2.3, i.e. using the NIST database [5]. The *standard heats of reaction* were computed by the heats of formation always available in [5] and are reported in table 5.

With these arrangement the chemical heat flux become:

$$q_{chem} = \sum_i^{N_{reac}} \left(\sum_{prod} \frac{M_{m,prod}}{M_{m,c}} \frac{\nu_{prod}}{\nu_c} \int_{T^\circ}^{T_w} c_p(T)dT + \Delta H_{reac}^\circ - \sum_{reag} \frac{M_{m,reag}}{M_{m,c}} \frac{\nu_{reag}}{\nu_c} \int_{T^\circ}^{T_w} c_p(T)dT \right) \dot{m}_{c,i}$$

Here the dependence between SHB and SMB can be seen in the base material reaction rates $\dot{m}_{c,i}$ which govern the species mass fluxes.

Since the base material is a reactant for it results:

$$\frac{M_{m,i}}{M_{m,c}} \frac{\nu_i}{\nu_c} = 1$$

Hence its contribution to chemical heat flux, if a constant ablative material specific heat is assumed, is:

$$-\dot{m}_c \int_{T^\circ}^{T_w} c_p(T)dT = \dot{m}_c\, c_{p,c}\, (T^\circ - T_w) = \rho_c\, c_{p,c}\, \dot{e}\, (T^\circ - T_w)$$

Remembering that the convective heat transfer used is:

$$q_{cond} = \rho_c\, c_{p,c}\, \dot{e}\, (T_w - T_o)$$

If the nozzle initial temperature T_o is close to the standard reference temperature T° then in the SHB the conductive heat computation can be neglected with the enthalpy difference between the wall and the standard conditions.

4.2.4 *Phenomena equation set*

The surface heat balance allows to calculate the equilibrium wall temperature needed to solve SMB equation set, composed by N equations with N equal to the number of species considered, but the surface heat balance needs only five species concentrations.

The remaining $N-5$ species concentrations are needed because the partial pressure requires the *mole fraction*, while the diffusivity driving force requires *mass fraction* and hence the complete wall species concentration information is required in order to compute the mole fraction from the mass fraction and vice versa.

It must be noted also that the SMB equation set would be uncoupled if it weren't for the "blowing" terms which include the overall ablative material erosion rate and hence a single SMB would be function of the relative species concentration and temperature wall only.

The complete equation set that describes the ablation phenomena is composed by N species surface mass balance an one surface heat balance. The system unknowns are the N considered species concentrations and the operative wall temperature. The way this equation set was solved using a *MATLAB*® is described further in section 4.3.

4.2.5 *Diffusion limited and kinetics limited behaviour*

Equation 15 shows the balance between the species diffusive mass flux through the boundary layer and species reaction rate at the surface. The surface reaction rate depends on the species diffusion through the boundary layer and vice versa. In this interconnected balance two extreme behaviour can be figured: *diffusion limited* and *kinetics limited*.

If the surface reaction occurs quicker than the diffusion then is the latter phenomenon to control the surface erosion rate, hence the reaction mechanism is said *diffusion limited*, in this case the species wall concentration is normally low (close to zero).

If the diffusion rate through the boundary layer is higher than the chemical kinetics then the surface erosion is controlled by the kinetics. This is the case of *kinetics limited* reaction, which is characterized by a wall species concentration close to the one on the free stream.

From the considered reacting species, normally H_2O, OH and O result to be diffusion limited, while O_2 and CO_2 are kinetics limited. But this can obviously change with propellant composition, wall temperature and ablative material.

Species surface concentration is a good parameter to monitor in order to understand if the related reaction is diffusion o kinetics limited. Another good way to see that, is to impose two different wall concentrations and then compare the equivalent surface reaction rate. First the diffusivity mass flux due to a zero wall concentration is calculated along with the related ablative material mass flux (only diffusive reaction rate). Then the ablative reaction rate due to a wall concentration equal to the free-stream one is computed (only kinetics reaction rate). If the only kinetics reaction rate is lower than the

only diffusive one then the species reaction is kinetics limited, otherwise the reaction is diffusion limited.

Understanding if a species reaction is diffusion or kinetics limited explain how the non-equilibrium ablation model will behave with respect to a simpler equilibrium model, and if it's worth the effort. Since in this case the molecular oxygen is often kinetics limited and lead to highly exothermic reactions the non-equilibrium model help to reduce the gap between the predicted and effective erosion rates so to give a more accurate model.

4.3 MODEL IMPLEMENTATION

The non-equilibrium ablation model for non-charring ablative materials presented in the previous section has been implemented in a *MATLAB®* *function*. This function was though for purposes that require a fast throat erosion rate evaluation, such as a preliminary design phase. This turns particularly useful in the peculiar HRM thermal environment which varies during the engine operating time, and when different propellant formulations are evaluated.

4.3.1 *Function input*

The surface erosion rate evaluation require the knowledge of the free-stream thermochemical environment, the related heat transfer and the ablative material thermophysical properties and the way it interacts with the flow. These aspects needed to get the thermochemical ablation become input values for the developed *MATLAB®* *function*.

The thermochemical environment inputs are:

- Combustion chamber conditions as temperature T_{cc}, pressure p_{cc} and characteristic velocity $c^\star$ which allow to calculate local the local specific mass flux, temperature and then the related thermodynamic and transport properties;

- Free-stream chemical composition expressed as species mass fraction, used in diffusivity and thermodynamic and transport properties calculations;

- Propellant specific heat used for the calorically perfect gas approximation and the one-dimensional gasdynamics.

These data are almost entirely obtained from look-up tables generated using CEA. This and the way the thermodynamic and transport properties are

computed is described in chapter 2.

The convective heat transfer is described by the following inputs:

- Film coefficient α or *Stanton number*, used in the SHB and in the *Reynolds analogy* for the diffusivity (close to unity *Lewis number*). In the function the film coefficient is used and it's estimated using the *Bartz equation*;

- The adiabatic wall temperature T_{aw} which is calculated from the combustion chamber temperature and the introduction of the recovery factor. A recovery factor equal to 0.9 is used, it has been shown to be a good assumption at the throat.

The methods used to predict the convective heat transfer coefficient and its driving force are described in chapter 3.

The involved ablative material thermophysics properties are:

- Specific heat c_c, used to compute the steady state conductive heat transfer;

- Density ρ_c, directly involved in the relation between ablative material mass flux and surface erosion;

- The thermal conductivity λ, complete the set of properties require for the thermal diffusivity, which influences the in-depth thermal response.

Other effects concerning the ablative material is the chemical interaction with the gas which turns in the kinetics constants used in the chemical kinetics model described in section 4.2.

4.3.2 *Implementation: solution of the phenomena equation set*

The ablative phenomenon system of equation was presented in section 4.2.4. It's composed by non-linear equation and often the unknown variables are implicitly defined, this requires the use of numerical methods for the solution of systems of non-linear equations. The *MATLAB®* *function* `fsolve`, developed by *Mathworks*™, solves such systems, but unfortunately not this system, even using initial conditions close to the right solution, hence an *ad hoc* solver was created.

The key points in developing the solver are the following facts:

- For a given wall temperature the SMB equation set is easier to solve than the complete system.

- In particular if the "blowing" term of the SMBs are neglected the system results uncoupled;

- The SHB could be easily solved if the wall species concentrations were known, this also means that for a temperature the deviation from zero of the SHB could be evaluated;

- Once a erosion rate is obtained the film coefficient must be updated accordingly to the *blowing correction*.

Noted this, a step solution of the system, based on the assumption of the wall temperature, was adopted.

The SMB equation set is solved using a bisection method, which is a functions solver and not a systems solver. In order to use this method, with which the convergence is granted, the fact number two of the above list was used. The following steps summarize the SMB equation set solution for a given temperature:

1. An initial surface mass flux is assumed;

2. Since the overall surface mass flux is known it's possible to solve every single surface mass balance individually;

3. Two boundary value for the individual species concentration are taken, (during the first iteration these are zero and the free-stream concentration), a mid-value is then computed as third point;

4. In these points the deviation from zero of the modified SMB[5];

5. Two new boundary values are taken based on the deviations results (convergence model), this values are used in point 3 until convergence is reached;

6. With the convergence wall concentrations a more realistic mass flux value is calculated. This is used in point 2 where an outer iterative loop starts;

7. When the ablative material mass flux caused by every single species doesn't change within an assumed tolerance, the algorithm has converged and the wall species concentration for a given wall temperature is obtained.

This process has been intensively used in the in the solution of the complete system and hence it will be referred as *SMBs solver*.

The SHB is solved along with the complete system using the following algorithm:

---

5 With a previously computed or supposed overall ablative material mass flux.

1. Two boundary wall temperature values, initially assumed to be $300K$ and $3000K$, are taken. Then a middle value is computed;

2. For these three wall temperature values the *SMBs solver* is individually applied in order to get the related wall concentrations;

3. The deviation of the SHB is evaluated in the three points using the newly obtained set of values;

4. Based on the deviations obtained two new wall temperatures boundary values are determined and used in point 1 until the convergence is reached.

With this algorithm it's possible to obtain the wall concentrations and temperature, the convergence is granted since it's based on the bisection method.

Once the wall temperature concentrations and temperature are obtained, the surface reaction rate is once again computed and then the blowing correction parameter can be calculated. With the new convective heat transfer coefficient the procedure to solve the complete system is restarted since the blowing correction variation is within a certain tolerance.

Only then the effective erosion rate that accounts for the blowing effect is obtained.

4.3.3 *Function output*

The *MATLAB® function* was implemented to be used in purposes that require a fast evaluation of the throat erosion rate. This is indeed the main output of the function along with the wall temperature. Other useful outputs are the individual species erosion rate and the blowing correction coefficient.

4.4 validation

In order to understand if the developed function correctly described the ablation phenomena, it has been subjected to a series of validation analyses. Most validations involved a comparison with the data in the paper published by *D. Bianchi and F. Nasuti* in [12].

D. Bianchi and F. Nasuti applied the non-equilibrium ablative model previously presented as an ablative boundary condition in a CFD analysis. This surely grant a more accurate prediction of the erosion rate since the method involve less hypotheses.

In [12] the BATES nozzle configuration is adopted as case study. This nozzle configuration was described in chapter 3 and for it a CFD analysis was carried out along with the application of the *Bartz equation* which is the main method used to predict the convective heat flux.

The BATES motor acronym of BAllistic Test and Evaluation System is a test motor that has been developed by the USAF during the late period of the 1960s decade and early 1970s. The aim of this research program was the study chamber environment of solid propelled rocket motors with different operating conditions and propellants formulation. This in order to predict a wide spectrum of combustion chamber conditions for the large solid rocket motors at the time under development.

The intensive quantity of experiments conducted on the motor produced a lot of data about the nozzle, which insert was realized in graphite. The erosion related data are a good basis to validate a thermochemical ablation model.

Nozzle geometric parameters and geometry are presented in table 2 and figure 9.

4.4.1 *Validation # 1*

The first validation consisted in determining the erosion rate for a given propellant formulation and then compare it with the one reported in reference [12]. The erosion rate was computed for three different propellant formulations resulting from the reaction between *WAX* fuel and H_2O_2 90% pure, N_2O and LOX[6] as oxidizer. The relative combustion chamber condition (composition and temperature) were obtained from table 3 in [12] and are reported in table 6 here.

Propellant	T_{cc}	H_2O	CO_2	OH	O	O_2	CO	N_2	NO
$WAX - LOX$	3469	20.66	28.70	7.45	3.00	13.12	26.49	0	0
$WAX - H_2O_2$	2946	59.57	23.44	3.93	0.42	5.31	6.85	0	0
$WAX - N_2O$	3231	9.37	13.54	2.47	0.85	4.33	10.37	56.45	2.38

Table 6: Combustion chamber conditions for validation # 1, temperatures are in Kelvin while species concentrations are percentual mass fraction, [12]

---

6 Liquid Oxygen

With these data a film coefficient has been calculated at the throat using the *Bartz equation*, a recovery factor of 0.9 was used for the adiabatic wall temperature. A density of 1830 kg/m^3 was used for the bulk graphite.

Then the *ablation MATLAB® function* was used to calculate the erosion and the wall temperature and these were compared with the one reported in the reference. Validation results and comparison are presented in figure 22 and table 7.

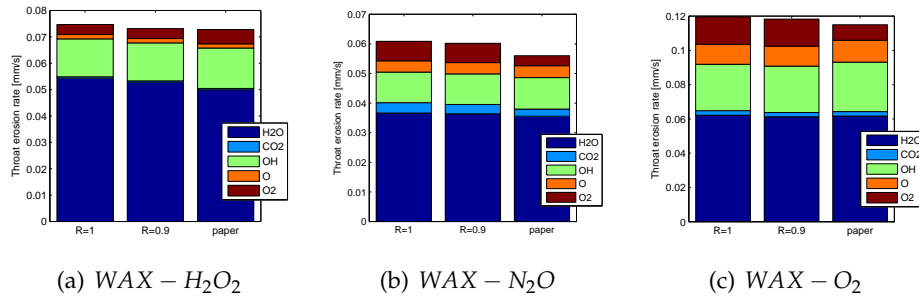(a) $WAX - H_2O_2$ (b) $WAX - N_2O$ (c) $WAX - O_2$

Figure 22: Bar diagrams of the thermochemical erosion for the three considered propellant formulations

Bar diagrams that describe the individual species contributions to the total throat erosion rates are reported in figure 22. Every bar diagram consist of three columns (bars), the first one report the calculated results obtained using a unity recovery factor, the second one shows the calculations made with a recovery factor equal to 0.9 and the third bar is the one reported in the reference which calculation involved the use of a more accurate CFD computer program.

The first thing that catch the eyes is that the difference between the $R = 0.9$ and $R = 1$ is very small compared to the difference between the computed results and the ones reported in the reference. The second thing that can be noted is that in most cases the differences between the calculation and the reported results are due to the behaviour of the O_2 and H_2O which are the most authoritative species. In fact H_2O gives the highest contribution to the erosion allowing to mitigate part of the incoming heat since the related heterogeneous reaction is highly endothermic. While O_2 which is normally present in higher concentrations than the atomic oxygen reduce the effectiveness of H_2O and other species giving a exothermic contribution to the overall endothermic wall reaction. That's why the *WAX*-LOX propellant formulation gives an higher erosion than the other: the residual O_2 free-stream concentration is higher.

In table 7 the numerical value of the erosions shown in figure 22 are reported. Here the quantitative evaluation of the model accuracy can be made.

	H_2O_2		N_2O		LOX	
	function	paper	function	paper	function	paper
H_2O	52.8	49.9	36.4	35.6	61.2	61.6
CO_2	0.54	0.51	3.15	2.41	2.52	2.6
OH	14.4	15.3	10.4	10.6	27.1	28.9
O	1.65	1.6	3.81	4.03	11.7	12.8
O_2	3.77	5.4	6.5	3.36	15.8	9.1
$\dot{e}\ [\mu m/s]$	73.2	73	60.2	56	118	115
$T_w\ [K]$	2183	2191	2500	2478	2405	2441

Table 7: Thermochemical erosions in validation # 1

The average relative difference between the calculation and the paper results is 3.46%, which is quite good considering the discrepancies previously detected in the results. Also the wall temperature results to be accurate, the average difference is 22 K relatively speaking less than 1%.

Another thing to note is the behaviour difference between the erosions obtained with H_2O_2 and N_2O. In particular N_2O cause a higher wall temperature than H_2O_2 but also a lower erosion rate. This is mainly caused by the overall presence of reacting species which for N_2O is thinned by the high nitrogen content, leading to a higher wall temperature where the H_2O reaction rates outweigh the negative effects of the O_2 reacting species. In this case higher wall temperature and low reacting species concentrations produce a beneficial effect.

From table 7 results that the H_2O_2 erosion rate prediction is more accurate than the one obtained for N_2O and LOX. How can be seen in figure 22, this is probably caused by the fact that the O_2 contribution is more close to the one predicted in the paper contrary to what happens for the N_2O and LOX erosion predictions, where the molecular oxygen results are not as accurate.

So to conclude, given the combustion chamber conditions reported in [12] and table 6, the erosion rate estimates computed using the developed *ablation MATLAB® function* are really close to the results reported in the reference paper [12], nonetheless some discrepancies were found in the individual reactive species contributions, but these are small if compared by the difference between the methods used to determine the throat erosion rates.

Since the accuracy of the *ablation MATLAB® function* has been shown for different oxidizers but single operating conditions, the next validation step is to demonstrate the accuracy with variable combustion chamber conditions, in particular varying the oxidizer to fuel ratio. This validation was done for the same three oxidizers discussed in the first validation (H_2O_2, N_2O and LOX) but the fuel used this time is HTPB[7], in order to compare the results with the trends reported in figure 23.
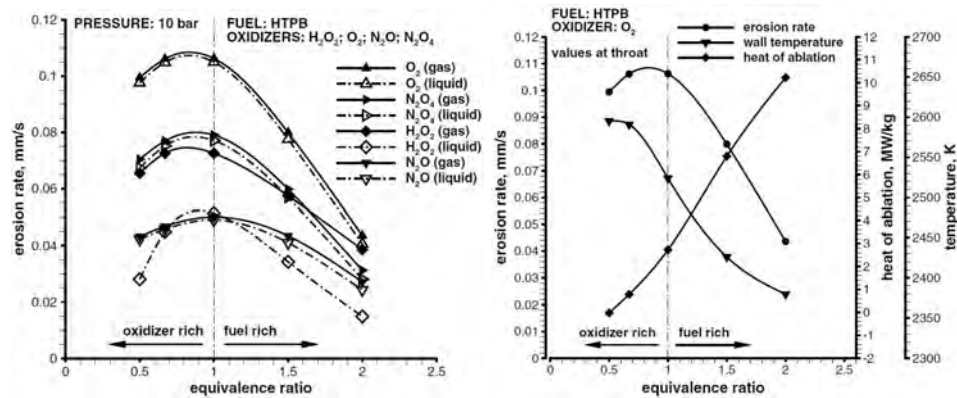

Figure 23: Erosion rates and other ablation results varying the o/f ratio, [12]

Figure 23 left side shows the trends of surface erosion rates with the variation of the *equivalence ratio*[8] for different oxidizer but the same HTPB fuel. These trends should be the results of this validation using the developed *ablation MATLAB® function*. Figure 23 right side shows, other than the erosion rate, the wall temperature and the heat of ablation related to the variation of the *equivalence ratio* for the HTPB-LOX propellant formulation.

Here the results will be presented for the HTPB-H_2O_2 first, followed by HTPB-N_2O and HTPB-LOX. In order to get the variable combustion chamber composition, a set of CEA based look-up table were used[9].

The HTPB-H_2O_2 stoichiometric reaction is:

$$C_{7.08}H_{10.65}N_{0.06}O_{0.22} + 23.24\ H_2O_{1.83} \rightarrow 7.08\ CO_2 + 28.56\ H_2O + 0.03\ N_2$$
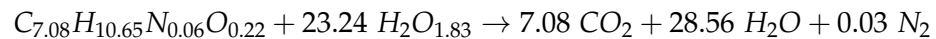
The relative stoichiometric oxidizer to fuel ratio $(o/f)_{sto}$ results equal to 7.35 which is also in the optimum I_{sp} operative range for the propellant

---

7 Hydroxyl-terminated polybutadiene

8 In reference [12] the fuel to oxidizer equivalence is adopted this is defined as $\phi = \frac{(o/f)_{sto}}{o/f}$

9 The way these look-up tables were obtained is described in chapter 2

formulation. The HTPB exploded formula and the relative heat of formation
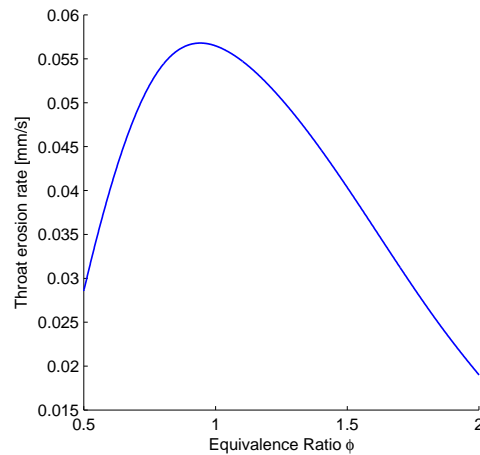were obtained from [14].

Figure 24: Calculated erosion rate trend due to a variation of the oxidizer to
fuel ratio for the HTPB-H_2O_2 propellant formulation

In figure 24, the erosion rate trend for a variable o/f is shown. The obtained
results are similar to the H_2O_2 (*liquid*) in figure 23a.

Let's consider the differences between this comparable trends:

- The calculated trend erosion rates are slightly higher than the ones
  reported in the reference paper;

- The maximum erosion rate occurs for a oxidizer rich mixture as happens
  in the reference, both maximum are close to $\phi = 0.9$. The calculated
  maximum erosion relative error is close to 8%.

- For $\phi = 0.5$ a value of $29\frac{\mu m}{s}$ is calculated while the reported one is
  approximatively $27\frac{\mu m}{s}$ which corresponds to a 7.4% over-predictive
  error;

- For $\phi = 2$ a value of $18\frac{\mu m}{s}$ is calculated while the reported one is
  approximatively $17\frac{\mu m}{s}$ which corresponds to a 6% over-predictive error.

In figure 25 a series of ablation related results are reported.

Figure 25a shows the free-stream mole fractions of the reacting species,
here H_2O is the main reaction product, it forms from the combustion and the
decomposition of the hydrogen peroxide, the latter is also the cause of the
molecular oxygen increase for low equivalence ratios.

Figure 25b shows the computed wall temperature, the combustion chamber
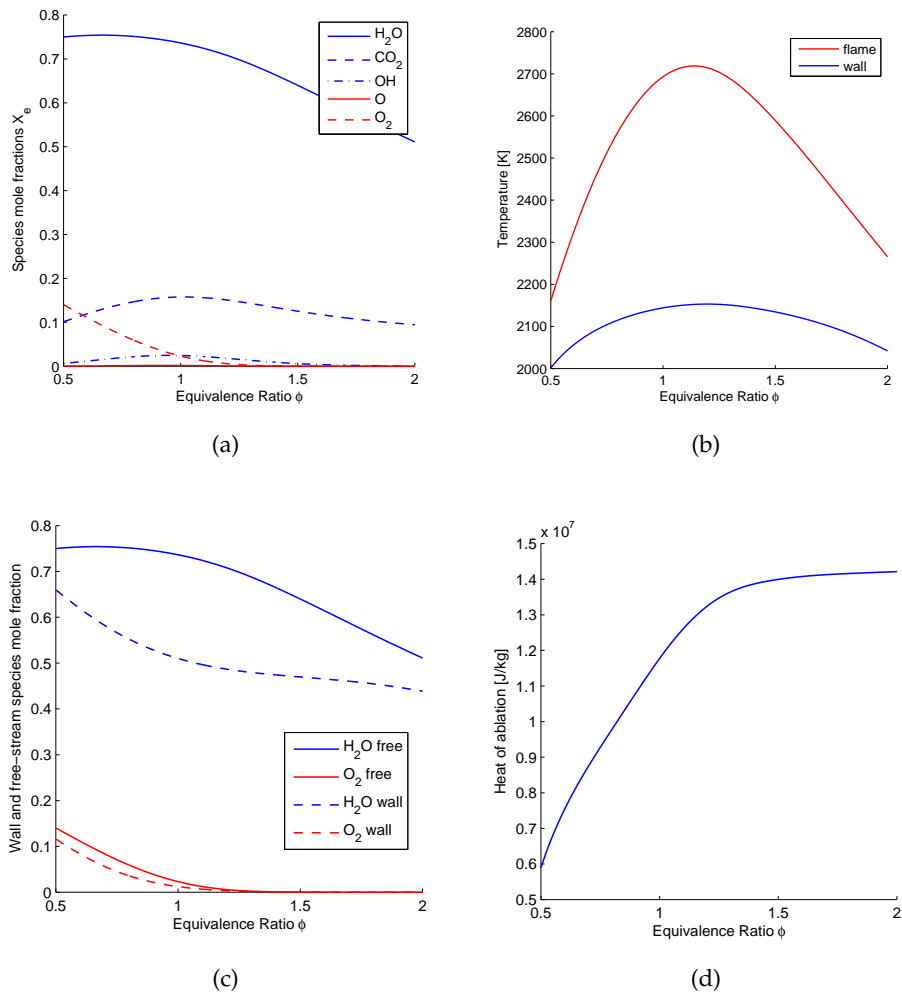temperature obtained with CEA and intrinsically the relation between the

Figure 25: Other ablation phenomena results by varying o/f, for the HTPB-H_2O_2 propellant formulation

two. The maximum wall temperature occurs at an equivalence ratio close to the one at which the maximum combustion chamber temperature occurs.

Figure 25c shows the wall and free-stream mole concentrations of H_2O and O_2 which produce the highest positive and negative contribution to the erosion rate. Here the *kinetics limited* behaviour of the molecular oxygen reaction can be seen.

Figure 25c shows how the heat of ablation varies with the equivalence ratio. In particular a reduction of the effectiveness occurs for an oxidizer rich propellant, this is mainly due to the higher content of molecular oxygen and lower wall temperature where the O_2 reaction rate increase with respect to the H_2O one.

For the HTPB-N_2O the stoichiometric reaction is:

$$C_{7.08}H_{10.65}N_{0.06}O_{0.22} + 19.26\ N_2O \rightarrow 7.08\ CO_2 + 5.33\ H_2O + 19.29\ N_2$$
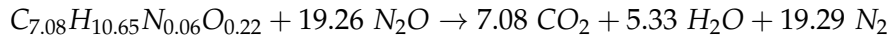
This implies a stoichiometric oxidizer to fuel ratio $(o/f)_{sto}$ of 8.56, which is higher than the theoretically optimum I_{sp} operating o/f of 7.2.
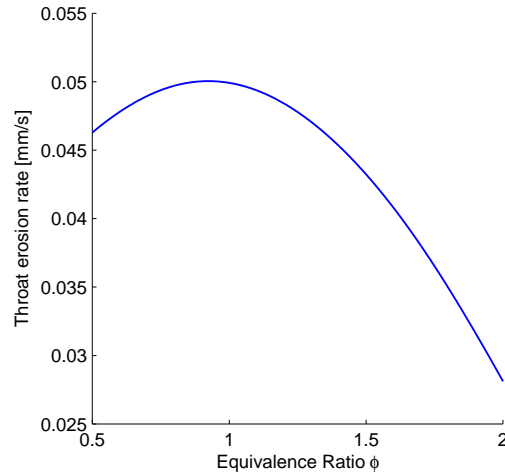

Figure 26: Calculated erosion rate trend due to a variation of the oxidizer to fuel ratio for the HTPB-N_2O propellant formulation

In figure 26 the throat erosion rate trend for different oxidizer to fuel ratios is shown. The obtained results agree well with the one reported in figure 23a, anyway few differences are present:

- The maximum erosion rate occurs for the same o/f, close to the stoichiometric one, a relative error lower than the 6% is detected for the maximum erosion rate values;

- For $\phi = 2$ a value of $27\frac{\mu m}{s}$ is calculated while the reported one is approximatively $25\frac{\mu m}{s}$ which corresponds to a 8% over-predictive error;

- For $\phi = 0.5$ a value of $46\frac{\mu m}{s}$ is calculated while the reported one is approximatively $43\frac{\mu m}{s}$ which corresponds to a 7% over-predictive error.

It's important to note that for normal o/f operative ranges, which reasonably will be close to the optimum I_{sp} oxidizer to fuel ratio equal to 7.2, the mixture results to be fuel rich. In these conditions the throat erosion rates estimated with the *ablation MATLAB$^{\circledR}$ function* are quite accurate.

A series of results that can be useful to understand the discrepancy between the calculated trend and the one reported in [12] are shown if figure 27.
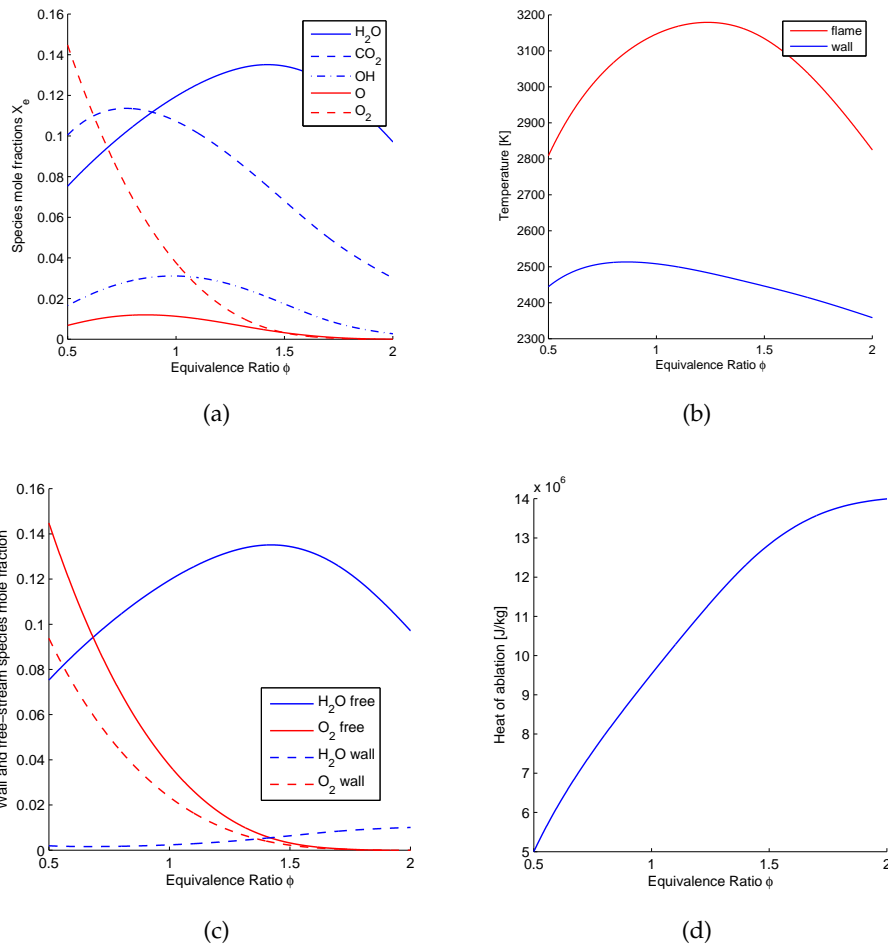
Figure 27: Other ablation phenomena results by varying o/f, HTPB-N_2O propellant formulation

Figure 27a shows how the reacting species mole fractions change varying the o/f, for a fuel rich mixture the H_2O and OH, which are "benign", concentrations are higher than the others, but with the decrease of the equivalence ratio $\phi \approx 0.5$ the O_2 concentration increases notably, up to exceed the H_2O concentration. This amount of molecular oxygen comes from the N_2O decomposition reaction which prevails for low equivalence ratios. Another important fact is that the overall reacting species concentration is low compared with the one usually found in HRM, this is due to the high concentration of N_2 that forms during the nitrogen oxide decomposition and leads to the higher wall temperatures.

Figure 27b shows the wall and combustion chamber temperatures. The fact that the maximum wall temperature doesn't match with the combus-

tion chamber maximum suggests that a negative effect due to the ablation mechanism occurs.

Figure 27c shows wall and free-stream mole fractions of the H_2O and O_2 reacting species. Here the *kinetics limited* nature of the O_2 reaction and the *diffusion limited* nature of the H_2O reaction can be seen clearly.

Finally figure 27d shows the computed heat of ablation trend which effectiveness decrease notably for low equivalence ratios which means higher o/f and hence molecular oxygen content due to nitrous oxide decomposition. This effectiveness reduction of the ablation mechanism can be identified as the cause why the wall and combustion chamber temperature maximums occur at different o/f.

For the HTPB-LOX the stoichiometric reaction is:

$$C_{7.08}H_{10.65}N_{0.06}O_{0.22} + 9.64\ O_2 \rightarrow 7.08\ CO_2 + 5.33\ H_2O + 0.03\ N_2$$
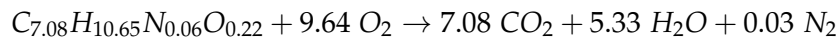
The relative stoichiometric oxidizer to fuel ratio $(o/f)_{sto}$ is equal to 3.12 which is once again higher than the optimum I_{sp} operating o/f value of 2.4 for this propellant formulation.
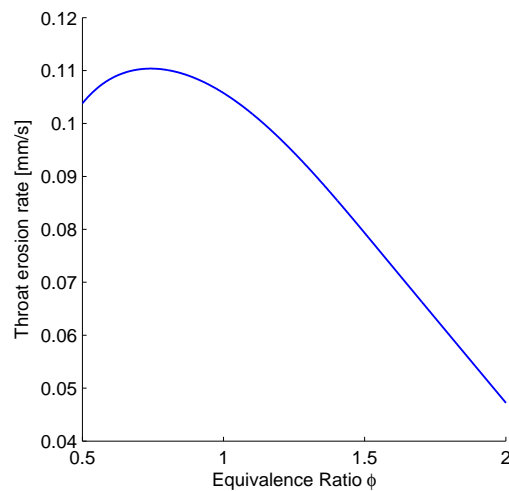
Figure 28: Calculated erosion rate trend due to a variation of the oxidizer to fuel ratio for the HTPB-LOX propellant formulation

Figure 28 shows the throat erosion rate trend with the variation of the o/f. Once again the computed results agree with the one reported in figure 23a:

- The calculated maximum throat erosion rate seems to occur at a slightly higher o/f than the one reported in figure 23a, a value of $111\frac{\mu m}{s}$ is calculated, while the reported one is approximatively $107\frac{\mu m}{s}$, leading to a relative error lower than the 4%;

- For $\phi = 0.5$ a value of $104\frac{\mu m}{s}$ is calculated while the reported one is approximatively $98\frac{\mu m}{s}$ which corresponds to a 6% over-predictive error;

- For $\phi = 2$ a value of $46\frac{\mu m}{s}$ is calculated while the reported one is approximatively $42\frac{\mu m}{s}$ which corresponds to a 9.5% over-predictive error.

It must be noted that optimum operative point for a hybrid motor with a HTPB-LOX propellant formulation occurs at oxidizer to fuel ratio equal to 2.4 i.e. with a fuel rich mixture where the throat erosion rate values computed with *ablation MATLAB® function* are accurate.
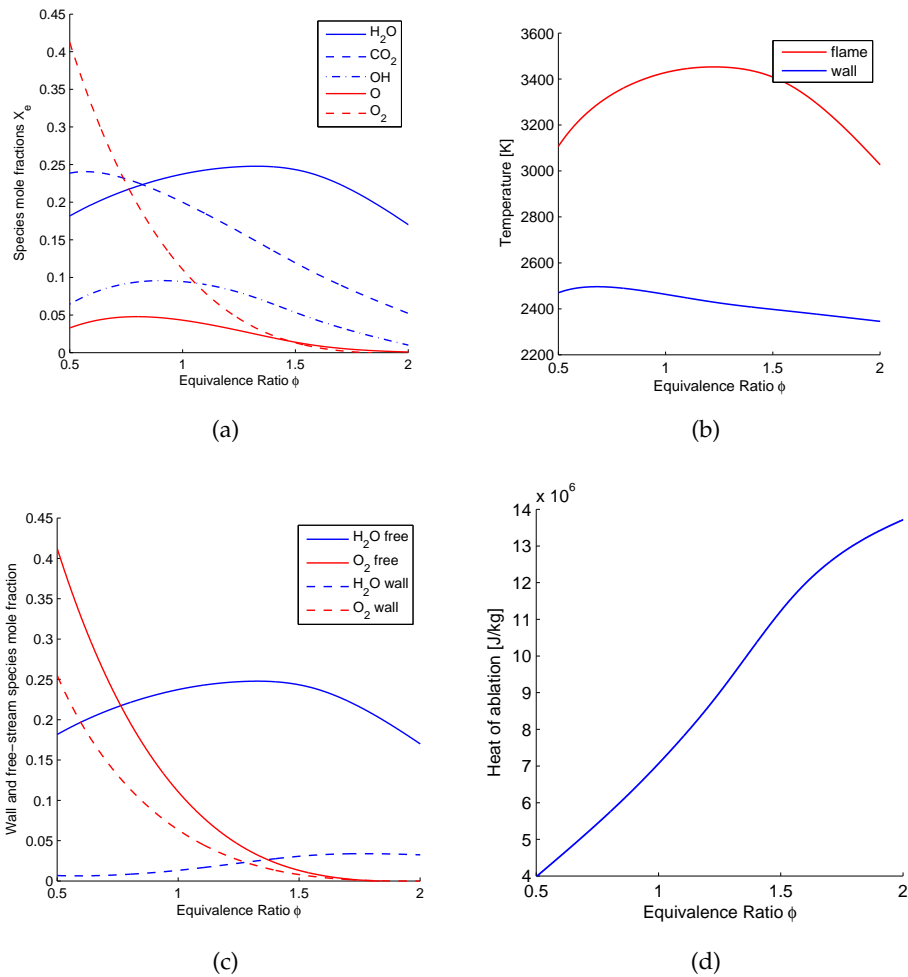

Figure 29: Other ablation phenomena results by varying o/f, HTPB-LOX propellant formulation

Figure 29 contain a set of trends that can be compared with the values reported in figure 23b.

Figure 29a shows the reacting species free-stream mole fractions obtained with CEA. The results are analogous with the one of figure 27a, but this time the oxidizer itself is molecular oxygen. This implies a much higher O_2 concentration for the exothermic reaction and hence a reduced overall heat of ablation.

Figure 29b shows the flame temperature for the propellant formulation obtained with CEA and the computed wall temperature. The calculated wall temperature trend is analogous to the one reported in figure 23b, but values for low equivalence ratios are lower than the reported one. This effect occurred also in the first validation, how can be seen from figure 22 and table 7.

Figure 29c shows the free-stream and wall concentrations of H_2O and O_2 reacting species. The H_2O reaction appears to be *diffusion limited*, while the O_2 reaction seems to be *kinetics limited* even if the diffusion controlled reaction mechanism is evident.

Figure 29d shows the heat of ablation trend for different o/f, this is similar to the one reported in figure 23b, but results to be higher. The ablation effectiveness decrease for lox equivalence ratio.

The fact that the computed heat of ablation results to be quite higher than the one reported in figure 23b can be associated with a conductive heat matter. In [12] a conductive heat flux of about $40 - 50\%$ of the incoming convective heat transfer is reported while in the calculations made the conductive to convective heat fluxes ratio was around the $10 - 25\%$ range. This discrepancy disagrees with the results obtained in the first validation where the reported wall temperature and the erosion rate errors were low. The only way for this to be possible is that both the estimated convective and heat transfer were both wrong at the same extent.

The calculated throat erosion rates trends result to be quite accurate. For all the propellant formulations the evaluated relative errors result to be over-predictive and lower than the 10%.

The small differences between the erosion trends can be attributed to:

- Different combustion chamber thermochemical data from the one utilized in the reference paper, could be due to little differences in the reactant formulation;

- Errors relative to the method used to estimate the film coefficient, which are discussed in chapter 3;

- Discrepancies about the heat of reaction reported in figure 19;

- The diffusion model adopted, *Reynolds analogy* for close to unity *Lewis numbers* was used ($Le = 1$ was assumed) and the uniform diffusion coefficient hypothesis was introduced.

4.5 RESULTS

The developed *ablation MATLAB® function* results to be less accurate than the CFD based model presented by *D. Bianchi and F. Nasuti* in [12], but it is surely faster. These two characteristics fit well with preliminary design throat erosion rate evaluation, in particular for the following purposes:

- Evaluation of the performance variation due to throat area increase;

- Thermal protection preliminary design, and nozzle weight evaluation.

During these evaluations the *ablation MATLAB® function* can be used in different ways:

- The function can be directly used in a code where the convective heat flux and other parameters are computed;

- An ablation look-up table can be generated, if some phenomenon independent variables are identified;

- Similarly to what is done with the look-up table an interpolating function of some phenomenon independent variables can be generated.

During the look-up table or interpolating function generation process it is possible to merge the *ablation function* with the convective heat transfer model adopted, so to obtain a more user friendly look-up table or interpolating function since the wall heat flux estimate is contained implicitly.

The phenomenon significant independent variables must be identified first if such interface models are desired. In chapter 4 the ablative model was presented along with the required inputs for the ablative function, these are a good start point to individuate the variables. The required inputs were:

- p_{cc} combustion chamber pressure;

- T_{cc} combustion chamber temperature;

- Y_e free-stream chemical composition;

- μ_e, λ_e and $c_{p,e}$ thermodynamic and transport properties;

- α film coefficient and T_{aw} adiabatic wall temperature;

- c_c ablative material specific heat;

- ρ_c ablative material density.

The combustion chamber temperature is determined with the CEA computer program and is a function of the combustion chamber pressure p_{cc} and the propellant formulation which in turn is identified by the o/f and the oxidizer and fuel type. The same is true for free-stream chemical composition.

The thermodynamic and transport properties, μ_e, λ_e and $c_{p,e}$, are function of both local static temperature and chemical composition which in turn depend from the combustion chamber pressure and the oxidizer to fuel ratio.

The ablative material density and specific heat are both independent variables, but it must be noted that while the density can vary significantly and directly affects the erosion rate, the specific heat has a lower effect on the erosion and hence can be considered a constant value.

Hence by merging the ablation model with the chemical equilibrium code and the thermodynamic and transport properties functions of temperature, the throat erosion rate become the following function:

$$\dot{e} = \dot{e}\left(p_{cc},\ o/f,\ \rho_c,\ \alpha,\ T_{aw}\right)$$

Here the adiabatic wall temperature can be expressed as a function of the combustion chamber temperature using the recovery factor definition:

$$T_{aw} = T_e + R\left(T^\circ - T_e\right)$$

The *Bartz equation* (equation 11) at the throat is equal to:

$$\alpha = \frac{C}{D_{th}^{0.2}}\left(\frac{D_{th}}{R_{c,th}}\right)^{0.1}\frac{\mu_e^{0.2}\,c_p}{Pr^{0.6}}\left(\frac{p_{cc}}{c^\star}\right)^{0.8}$$

Considering that the ratio $\frac{D_{th}}{R_{c,th}}$ is normally close to 1 and that the 0.1 power of the ratio is present in the film coefficient function, this term can be neglected in this evaluation.

$c^\star$, which is the rocket characteristic velocity, is determined using CEA end hence is a function of p_{cc} and o/f. The same is true for the thermodynamic and transport data and the *Prandtl number*.

The throat diameter is an independent variable along with p_{cc} and o/f.

Hence the film coefficient can be expressed as a function of D_{th}, p_{cc} and o/f:

$$\alpha = \alpha\left(D_{th},\ p_{cc},\ o/f\right)$$

Merging the ablation and film coefficient functions results that the throat erosion rate in a hybrid rocket motor is a function of p_{cc}, o/f, D_{th} and ρ_c, which are independent variable:

$$\dot{e} = \dot{e}\left(p_{cc},\ o/f,\ D_{th},\ \rho_c\right)$$

The most general and valid procedure now would be a look-up table generation, which data can be interpolated different ways, or a dimensional analysis and the definition of dimensionless groups how is done in [15].

In traditional erosion evaluation methods, used in SRM environment, the following simple equation has been used to scale the erosion data:

$$\dot{e} = K \frac{p_{cc}^{0.8}}{\rho_c \, D_{th}^{0.2}}$$

which involve a proportional dependence of the erosion rate with the convective heat flux.

For HRM obtaining such a simple scaling equation is quite more complicated because of the contribution due to o/f variations. Anyway it is possible to obtain a simple interpolating function for a given oxidizer to fuel ratio.

Considering a *WAX-H_2O_2* 90% *pure* propellant combination operating at stoichiometric conditions ($o/f = 7.35$) a possible interpolating function is:

$$\dot{e} = 1.0732 \cdot 10^{-6} \frac{p_{cc}^{0.795}}{\rho_c^{1.01} D_{th}^{0.16}} \tag{18}$$

This function was obtained considering the individual contribution to the erosion for the p_{cc}, D_{th} and ρ_c independent variables. Even if no combined contributions were considered the obtained interpolating function doesn't lead to excessive errors.

The nominal values[10] for the combustion chamber pressure, throat diameter and material density are 15 *bar*, 0.1 *m* and 1900 kg/m^3 respectively.

Figure 32 shows different trends obtained using the ablation function and the interpolating function (eq. 18).

Figures 32a, 32b and 32c show the individual variable variations used in determining the equation 18 power exponents. Values from 5 to 50 *bar* were considered in evaluating the pressure effect on the erosion, the throat diameter was varied from 1 *cm* to 1 *m* and densities between 1500 and 2200 kg/m^3 were considered.

Figures 32d, 32e and 32f show other trends obtained for non nominal values of the p_{cc}, D_{th} and ρ_c independent variables, it can be seen that the interpolating function still gives accurate results.

From equation 18 the following main facts emerge:

- The throat diameter exponent is lower than 0.2, and since this variable appears only in the *Bartz equation* the erosion rate computed using equation 18 is not proportional to the heat flux;

---

10 Here nominal values means the values used in obtaining equation 18

- The ratio between the combustion chamber pressure exponent and the throat diameter one is higher than 4 which is the ratio reported in the *Bartz equation*, hence the pressure have a major influence in the ablation phenomena than the only relation with the film coefficient, this is attributable to the chemical kinetics contribution to the erosion.

Equation 18 has been shown to be a good interpolating function for $o/f = 7.35$, but it doesn't take into account of oxidizer to fuel ratio variations. In fact for different o/f the proportionality constant is not the only thing that changes, also the variables exponents are different.

Let's assume to use the following interpolating function:

$$\dot{e} = K\left(o/f\right) \frac{p_{cc}^{0.795}}{\rho_c^{1.01} D_{th}^{0.16}} \qquad (19)$$

which uses the stoichiometric power exponents but a different proportional constant for varying o/f.

Here the $K\left(o/f\right)$ function has been interpolated using the following third order polynomial:

$$K\left(o/f\right) = -2.264e - 6 + 8.802e - 7 \cdot o/f - 6.830e - 8 \cdot o/f^2 + 1.388e - 9 \cdot o/f^3$$

Which is valid from $o/f = 3.7$ and $o/f = 11$. This polynomial was obtained by normalizing the coefficient of the least squares interpolating polynomial shown in figure 30.
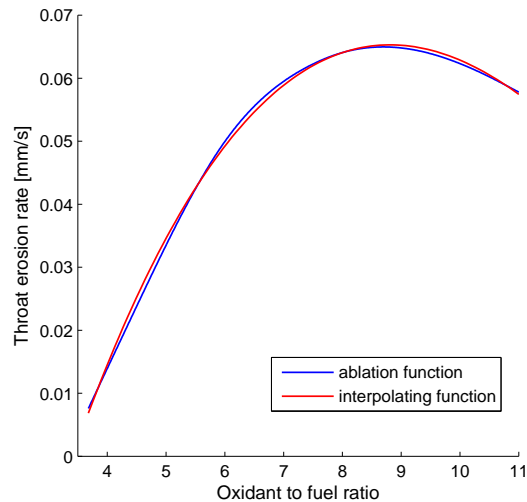

Figure 30: Throat erosion rate trend for varying o/f and nominal combustion chamber pressure and throat diameter

In figure 31 the trends obtained using the ablation function and equation 19 are reported. It can be noted that the error increases with the deviation of the operating conditions from the nominal ones. This means that function 19 can be used for a fast throat erosion rate evaluation during a hybrid rocket motor analysis where the combustion chamber pressure and the throat diameter variations are not too high.

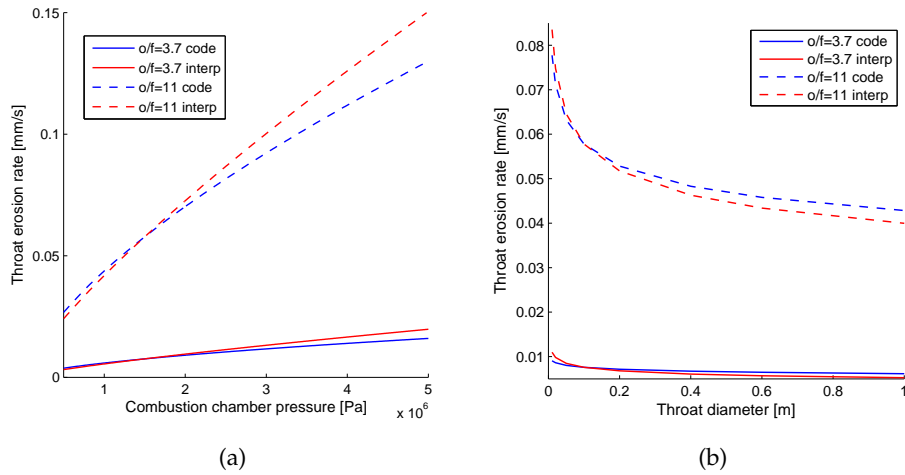(a)   (b)

Figure 31: Interpolating function results for non stoichiometric o/f

In experimental data scaling the operating conditions can be quite different, hence the suggested procedure would be to evaluate the erosion rate for the two different conditions using the ablation function and then use their ratio as scaling factor.
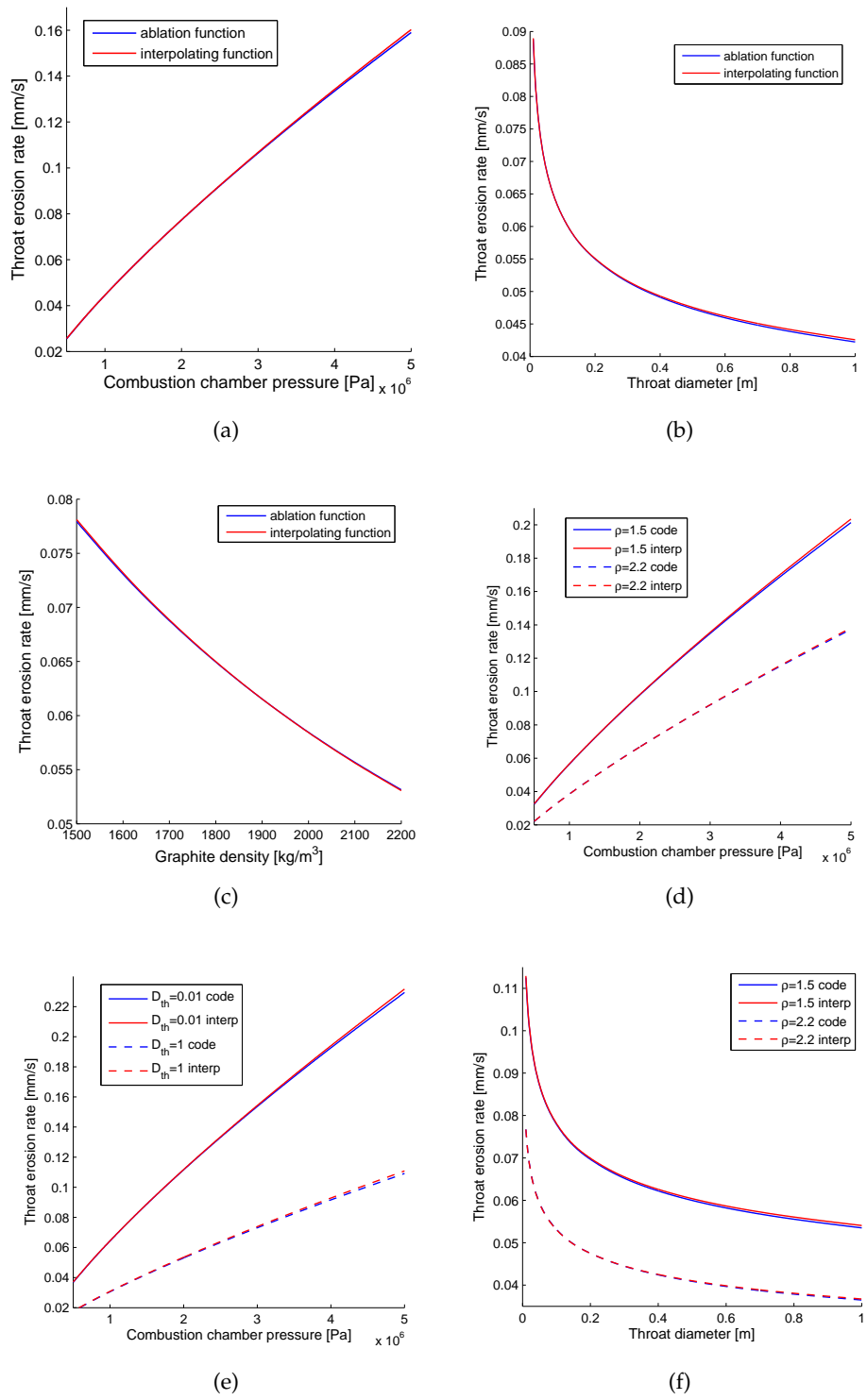
Figure 32: Interpolating function results for stoichiometric o/f

CONCLUSION

During the course of this thesis work a method to predict the throat erosion rate in hybrid rocket motors was implemented. This method involved the use of a non-equilibrium thermochemical ablation model, which turned particularly useful in obtaining an accurate estimate of the throat erosion. This model was limited to the modelling of non-charring ablative materials, which however are the most used in manufacturing of throat inserts.

The need for such method is required by the peculiar application of these ablative thermal protections, in fact the throat erosion rate in hybrid rocket motors results to be higher than the one obtained in solid rocket motors and is also characterized by the propellant formulation, which can vary from motor to motor and within a motor operating time.

In order to develop this method, different physics and chemical phenomena were studied and modelled, these involved: equilibrium chemical composition, thermodynamic and transport properties, convective and conductive heat transfer, gas phase diffusivity through the boundary layer, heterogeneous reaction at the surface and mass and energy balances.

These are also the phenomena involved in a nozzle aerothermal analysis, which is carried out with the following steps:

- Thermochemical environment characterization;

- Convective heat flux and diffusivity mass flux evaluation;

- In-depth thermal response evaluation with a surface thermochemical ablation model boundary condition.

THERMOCHEMICAL ENVIRONMENT CHARACTERIZATION

The first step of the ablative modelling procedure was the thermochemical environment characterization of the hybrid rocket motor, which consists in determining the combustion chamber chemical composition and temperature.

In this thesis work this step was achieved using the NASA's CEA computer program which has been developed by NASA Lewis Research Center and is based on the *Gibbs free energy* minimization.

CEA required inputs for the *rocket problem* are the propellent formulation and combustion chamber pressure and since these parameters normally vary, a look-up table based on the CEA program was generated for the combustion chamber chemical composition and temperature.

Using a self-developed look-up table generator based on CEA, different look-up table sets where obtained for the propellant formulations of interest

which were: *WAX-H$_2$O$_2$, WAX-N$_2$O, WAX-LOX, HTPB-H$_2$O$_2$, HTPB-N$_2$O* and *HTPB-LOX.*

Then the temperature dependent thermodynamic and transport properties of the individual species were computed using NIST fitting functions or interpolating functions obtained from NIST data. After this, for a given chemical composition, the mixture thermodynamic and transport properties were computed using the *mixing laws* presented in [3]. The computed thermodynamic and transport properties are: specific heat, viscosity and thermal conductivity.

During this step the CEA computer program allowed to get other useful data such as the theoretical characteristic velocity and nozzle thrust coefficients in frozen and equilibrium hypotheses.

HEAT AND DIFFUSIVITY MASS FLUXES EVALUATION

Once the combustion chamber thermochemical environment has been characterized it's possible to model the heat transfer. In this thesis work, only the convective and conductive components of the heat transfer were considered, while the radiation contribution has been neglected.

Two method to predict the convective heat transfer were used: the *Bartz equation* and the *ANSYS fluent* CFD computer program. Both of them where applied to the BATES motor nozzle configuration, since this configuration was used in the validating data of reference [12].

Even if two film coefficient trends were obtained for the BATES motor nozzle configuration, the data from the *Bartz equation* were used in the ablation model, since it was shown that the relative error between the trends can be accepted in order to get a faster estimate of the convective heat transfer describing parameters, which is a more important feature during the preliminary design.

The conductive heat flux was modelled using the steady state temperature profile for a movable coordinate system. This simplifying hypothesis allows to get the steady state conductive heat flux, that on the other hand can not be used when the *heat sink* effect of the nozzle can not be neglected, like in motors with a short burning time or ablative materials with high thermal conductivity. In these cases a transient in-depth thermal code must be coupled with the surface thermochemical ablation code.

After the convective heat transfer characterization the diffusive mass fluxes were modelled, this was achieved using the *Reynolds analogy* for close to unity *Lewis number* and the equal diffusive coefficients hypothesis.

In this step a non-equilibrium ablative model was implemented in order to estimate the throat erosion rate of graphite and carbon-carbon throat inserts, even if this procedure could have been applied to different non-charring ablative materials.

The heterogeneous surface chemical reactions kinetics model was taken from reference [12].

In order to obtain the erosion rate and the wall temperature, the N species surface mass balances and the surface energy balance were solved using an *ad hoc* solver based on the *bisection method*.

The implemented non-equilibrium thermochemical ablation model then was validated, along with the method used to obtain the heat and mass fluxes, using the data reported in [12]. During this validation procedure the BATES motor nozzle configuration was used to compute the convective heat transfer and the ablative material was assumed to be a bulk graphite of density equal to 1.83 g/cm^3. Two different validations were carried out.

The first validation aimed to show the accuracy of the developed method in predicting the throat erosion rate and wall temperature starting from a given free-stream composition and adiabatic flame temperature (The CEA computer program wasn't used during this validation). This validation was carried out for the *WAX-H$_2$O$_2$*, *WAX-N$_2$O* and *WAX-LOX* propellant formulations operating at stoichiometric oxidizer to fuel ratio, the relative combustion chamber composition and temperature was obtained from [12].

During this validation the throat erosion errors relative to the value reported in [12] were lower than the 5% with an average value of 3.5%, while the differences between wall temperatures were lower than 35K. This errors are low considering the difference between the method presented in this thesis and the one reported in [12]. It was also noted that the O_2 reaction was *kinetics limited* for all the propellant formulations, while the H_2O reaction resulted *diffusion limited* for the *WAX-N$_2$O* and *WAX-LOX* propellant formulations and *kinetics limited* for *WAX-H$_2$O$_2$*.

The second validation aimed to get the throat erosion rate trends for varying oxidizer to fuel ratio and compare them with the one reported in the reference paper. These particular trends are important in HRM since the oxidizer to fuel ratio can vary from motor to motor and within a motor operating time. This validation was carried out for the *HTPB-H$_2$O$_2$*, *HTPB-N$_2$O* and *HTPB-LOX* propellant formulations using again the BATES motor nozzle configuration.

In this validation the errors relative to the trends reported in the reference paper were lower than the 10%. There were slightly higher errors than the ones reported during the first validation, which indicates that additional

errors could have been introduced by the method used in determining the combustion chamber composition and temperature.

The relative errors obtained are acceptable during a preliminary analysis were the low computational time is more precious than a higher accuracy.

INTERPOLATING FUNCTION

In order to further reduce the computational time required to get a throat erosion rate estimate, the developed method was used to obtain an interpolating function similar to the one used in SRM throat erosion data scaling.

An interpolating function was obtained for the WAX-H_2O_2 propellant formulation at stoichiometric o/f which gave good results. It was also shown that the use of this interpolating function for different o/f leads to inaccuracies that increase for higher deviation of the motor operating parameters from the nominal ones. This means that the interpolating equation can be used for a fast throat erosion rate evaluation during a hybrid rocket motor analysis where the combustion chamber pressure and the throat diameter variations are not too high.

If the operation condition vary too much then the most rigorous way to obtain a throat erosion rate estimate would be the direct use of the implemented ablation model or a look-up table generation.

CONCLUSION

So to conclude a fast method to predict the throat erosion rate based on the non-equilibrium thermochemical erosion of non-charring ablative materials was implemented in $MATLAB^{\circledR}$ and validated along with the methods to predict the convective heat transfer and combustion chamber environment.

BIBLIOGRAPHY

[1] NASA Lewis Research Center.
Solid Rocket Motor Nozzles.
NASA Space Vehicle Design Criteria SP-8115.
June 1975.

[2] B.H. Prescott, Michael Macocha.
Nozzle Design.
AIAA Educational Series. Tactical missile propulsion.
Copyright 1996.

[3] Sanford Gordon & Bonnie J. McBride.
Computer Program for Calculation of Complex Chemical Equilibrium Composition and Application.
NASA Reference Publication 1311.
October 1994.

[4] George P. Sutton, Oscar Biblarz.
Rocket Propulsion Elements, 7^{th}edition
John Wiley & Sons.
Copyright 2001.

[5] *NIST Chemistry WebBook.*
NIST Standard Reference Database Number 69.
http://webbook.nist.gov/chemistry/
Copyright 2011.

[6] E. W. Lemmon, M. L. Hubert, M. O. McLinden.
Reference Fluid Thermodynamics and Transport Properties.
NIST Standard Reference Database 23, Version8.0.
Physical and Chemical Properties Division.
Copyright 2007.

[7] John D. Anderson Jr.
Fundamentals of Aerodynamics.
McGraw-Hill.
Third Edition.

[8] D.R. Bartz.
Turbulent Boundary-Layer Heat Transfer from Rapidly Accelerating Flow of Rocket Combustion Gasses and of Heated Air.
Advances in Heat Transfer, Volume 2.
Academic Press 1965.

[9] Prof. Manuel Martinez-Sanchez.
Lecture 7: Convective Heat Transfer: Reynolds Analogy.
Rocket Propulsion.

[10] Rashid A. Ahmad.
Convective Heat Transfer in the Reusable Solid Rocket Motor of the Space Transportation System.
ATK Thiokol Propulsion, AIAA-2001-3585.
July 8-11, 2001.

[11] Aerotherm Corporation.
USER'S MANUAL AEROTHERM CHARRING MATERIAL THERMAL RESPONSE AND ABLATION PROGRAM VERSION 3.
Aerotherm Report No. UM-70-14.
April 1970.

[12] Daniele Bianchi, Francesco Nasuti.
Numerical Analysis of Nozzle Material Thermochemical Erosion in Hybrid Rocket Engines.
JOURNAL OF PROPULSION AND POWER. Vol. 29, No. 3.
May–June 2013.

[13] W. A. Stephen, et al.
BALLISTIC MISSILE PROPELLANT EVALUATION TEST MOTOR SYSTEM.
AFRPL-TR-74-70 Air Force Rocket Propulsion Laboratory.
25 Nov 1974.

[14] Naminosuke Kubota.
Propellants and Explosives: Thermochemical Aspects of Combustion.
Wiley-WCH.
9 gen 2007.

[15] B. Evans, K.K. Kuo, E. Boyd and A.C. Cortopassi.
Comparison of Nozzle Throat Erosion Behaviour in a Solid-Propellant Rocket Motor and a Simulator.
AIAA 2009-5421.
2-5 August 2009,.

ACRONYMS

NASA   National Aeronautics and Space Administration

NIST   National Institute of Standard and Technology

USAF   United States Air Force

SRM   Solid Rocket Motor

HRM   Hybrid Rocket Motor

SMB   Surface Mass Balance

SHB   Surface Heat Balance

BATES   Ballistic Test and Evaluation System

CFD   Computational Fluid Dynamics

UDF   User Defined Function

CAD   Computer Aided Design

CEA   Chemical Equilibrium and Application

CMA   Charring Material Thermal Response and Ablation

ASCHAR   Axisymmetric Transient Heating and Material Ablation

EST   Equilibrium Surface Thermochemistry

HTPB   Hydroxyl-terminated polybutadiene

LOX   Liquid Oxygen

IRFNA   Inhibited red fuming nitric acid

GUI   Graphical User Interface

ACKNOWLEDGMENTS

I would first like to thank my family for their support during the years I spent at the University of Padua, without them this work and other personal achievement would not have been possible.

I would also like to thank my thesis committee members *Prof. Daniele Pavarin* and *Ing. Francesco Barato* of the CISAS hybrid propulsion group for their guidance as supervisors for the last six months.

Finally I want to thank my classmates, in particular *Diego Martignago* and *Stefano Torresan*, with whom I had the pleasure to work to some traditional and other less traditional projects during the last two years.

Vorrei ringraziare per primi i membri della mia famiglia per il loro aiuto negli anni che ho passato all'Università degli Studi di Padova, senza di loro questo lavoro di tesi e altri raggiungimenti personali non sarebbero stati possibili.

Vorrei inoltre ringraziare il Professor *Daniele Pavarin* e l'Ingegner *Francesco Barato* del gruppo di ricerca per la propulsione ibrida presso il CISAS per la guida che mi hanno fornito in quanto relatori per questo lavoro di tesi.

Infine voglio ringraziare i miei compagni di corso, in particolar modo *Diego Martignago* e *Stefano Torresan* con i quali ho avuto l'onore di lavorare ad alcuni progetti universitari, tradizionali e non, durante il corso di laurea magistrale.

Alessandro Ruffin - 20 Febbraio 2015